

# The Classic “Brown-Ring” Reaction in a New Medium: Kinetics, Mechanism, and Spectroscopy of the Reversible Binding of Nitric Oxide to Iron(II) in an Ionic Liquid

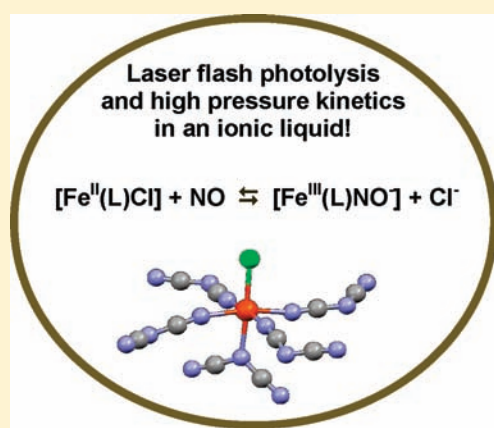
Svetlana Begel,<sup>†</sup> Frank W. Heinemann,<sup>†</sup> Grzegorz Stopa,<sup>‡</sup> Grazyna Stochel,<sup>‡</sup> and Rudi van Eldik<sup>\*,†</sup>

<sup>†</sup>Inorganic Chemistry, Department of Chemistry and Pharmacy, University of Erlangen-Nürnberg, Egerlandstr. 1, 91058 Erlangen, Germany

<sup>‡</sup>Faculty of Chemistry, Jagiellonian University, Ingardena 3, 30-060 Kraków, Poland

**S** Supporting Information

**ABSTRACT:** To elucidate the applicability and properties of ionic liquids (ILs) to serve as chemical reaction media for the activation of small molecules by transition-metal complexes, detailed kinetic and mechanistic studies were performed on the reversible binding of NO to FeCl<sub>2</sub> dissolved in the IL 1-ethyl-3-methylimidazolium dicyanamide ([emim][dca]) as a solvent. We report, for the first time, the application of laser flash photolysis at ambient and high pressure to study the kinetics of this reaction in an IL. The kinetic data and activation parameters for the “on” and “off” reactions suggest that both processes follow a limiting dissociative (D) ligand substitution mechanism, in contrast to that reported for the same reaction in aqueous solution, where this well-known “brown-ring” reaction follows an interchange dissociative (I<sub>d</sub>) ligand substitution mechanism. The observed difference apparently arises from the participation of the IL anion as a N-donor ligand, as evidenced by the formation of polymeric [Fe(dca)<sub>3</sub>Cl]<sub>x</sub>[emim]<sub>2x</sub> chains in the solid state and verified by X-ray crystallography. In addition, infrared (IR), Mössbauer, and EPR spectra were recorded for the monomeric reaction product [Fe(dca)<sub>5</sub>NO]<sup>3-</sup> formed in the IL, and the parameters closely resemble those of the {FeNO}<sup>7</sup> unit in other well-characterized nitrosyl complexes. It is concluded that its electronic structure is best described by the presence of a high-spin Fe(III) (*S* = 5/2) center antiferromagnetically coupled to NO<sup>-</sup> (*S* = 1), yielding the observed spin quartet ground state (*S*<sub>t</sub> = 3/2).



## INTRODUCTION

Ionic liquids (ILs) have been studied extensively as potential benign solvents for a wide range of chemical processes.<sup>1–4</sup> Because of their different tunable properties, such as density, viscosity, polarity, melting point, and solubility, they have found different applications in new technologies.<sup>5,6</sup> However, there is obviously still a lack of understanding of how these solvents actually influence or interact with substrates, since some groups have reported an increase or decrease in reactivity, or even a complete inhibition of a reaction.<sup>7,8</sup> Our goal is to quantify possible mechanistic changes and the origin of these changes when a typical reaction of a metal complex, extensively studied in conventional solvents before, is transferred into an ionic liquid. The time has come where ILs should not be employed on a trial-and-error basis, but rather on the basis of a well-founded chemical and mechanistic understanding. We recently reported on the significant effects of a series of ILs, including different anionic components, on substitution reactions of Pt(II) complexes.<sup>9</sup>

It is well-known that, generally, ILs greatly improve the solubility of gases, especially that of polar ones like carbon dioxide.<sup>10</sup> The reason for this is their specific inner structure with empty

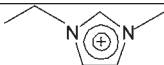
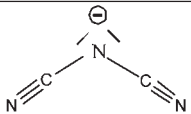
cavities between the cationic and anionic components. The formation of such cavities seems to be connected with the tendency of the ions to associate into aggregates, which appears to be a general feature of ionic systems at low densities.<sup>11</sup> More systematic investigations indicate that gas solubility is, on the one hand, an effect of the polarity and polarizability of a gas, and, on the other hand, depends on the nature and steric features of the cationic and anionic components, like acidity/basicity of the ILs and/or the fluorination of the cation or anion.<sup>12</sup> Thus, tailor-made ILs are also considered as storage media for harmful gases or as separation agents for gas mixtures.<sup>13</sup>

The reaction of nitric oxide (NO) with transition-metal ions plays an important role in environmental and biological processes.<sup>14</sup> This is partly related to the unique redox behavior of NO as a result of its radical character in the ground state. This results in the tendency of NO to bind to metal centers either as NO<sup>+</sup> or as NO<sup>-</sup>, such as in metmyoglobin where the Fe(III) center binds NO in the form of Fe<sup>II</sup>-NO<sup>+</sup>,<sup>15</sup> or in reduced vitamin B<sub>12</sub> where Co(II) binds NO in

Received: November 22, 2010

Published: March 23, 2011

Table 1. Structure and Physical Properties of the Ionic Liquid (IL) under Study

 1-ethyl-3-methylimidazolium [emim]	colour miscibility with water melting point [°C]	slightly yellow yes -21
 dicyanamide [dca]	viscosity (cP at 25 °C) density (g/cm <sup>3</sup> at 20 °C)	21 1.11

the form of  $\text{Co}^{\text{III}}-\text{NO}^-$ ,<sup>16</sup> respectively. Such interactions demonstrate the biological importance of NO, which was announced as “molecule of the year” in 1992.<sup>17</sup>

The interaction of NO with aquated Fe(II) is a reaction used as a spot test (brown ring test) for nitrate in introductory freshman laboratory courses. The details of the underlying reaction mechanism, with respect to the processes involved in the formation of the characteristic green-brown color of the  $[\text{Fe}(\text{H}_2\text{O})_5\text{NO}]^{2+}$  species, were studied extensively in our group.<sup>18</sup> Detailed spectroscopic and kinetic studies resolved the nature of the nitrosyl product, which is best described by the presence of high-spin Fe(III) ( $S = 5/2$ ) antiferromagnetically coupled to  $\text{NO}^-$  ( $S = 1$ ) yielding the spin quartet ground state ( $S_t = 3/2$ ), and clarified the mechanism of the “on” and “off” reactions, which follow an interchange dissociative ( $I_d$ ) ligand substitution process for both reactions.

We report here an extensive mechanistic analysis of the classical “brown-ring” reaction of iron(II) chloride with NO gas dissolved in an imidazolium-based ionic liquid, 1-ethyl-3-methylimidazolium dicyanamide ([emim][dca]). The structure and physical properties of the IL and its components under investigation are presented in Table 1.

The selected IL is among the best studied to date and was readily available. The purity of [emim][dca] was considered to be very important, since it was recently found in our group that even a very low concentration of an impurity can dramatically change the reaction mechanism.<sup>19</sup> The employed kinetic techniques enable a detailed insight into the nature of the underlying reaction mechanism in the selected IL. In addition, X-ray crystal structure determination to clarify the structure of the ferrous salt in the IL, and IR, Mössbauer, and EPR measurements on the nitrosyl reaction product helped to improve our understanding of the observations in the IL.

## EXPERIMENTAL SECTION

**Materials.** All chemicals used were of analytical-reagent grade and of the highest purity commercially available.  $\text{FeCl}_2$  anhydrous, purchased from Sigma–Aldrich, was used as a source for the Fe(II) solutions. NO gas (Praxair Deutschland GmbH & Co. KG, Bopfinger, purity 3.0) was cleaned from trace amounts of higher nitrogen oxides by passing it through concentrated KOH solution, an Ascarite II column (NaOH on silica gel, Sigma–Aldrich), and a phosphorus pentoxide column. Unless stated otherwise, all experiments were performed under an inert gas atmosphere.

**Synthesis and Purification of the Ionic Liquid (IL).** One batch of [emim][dca] was purchased from Io-Li-Tec GmbH & Co. KG, and another batch was synthesized in our laboratory in an effort to improve the purity of the IL. However, careful examination demonstrated that

both batches showed similar optical purity. The purchased IL was worked up in the following way to obtain the optical purity required for our spectroscopic investigations. First, it was stirred with activated charcoal (Norit A Supra) for 3–4 days. Afterward, it was dissolved in acetonitrile (Roth) and filtered slowly over a thick layer of silica gel (Aldrich/230–400 mesh/60 Å), allowing the impurities to be taken out. All further operations were performed under nitrogen atmosphere. The [emim][dca] had also to be cleaned of Na[dca] leftovers from the synthesis. Therefore, the liquid was dried under vacuum at 40 °C for 3–4 days and then a 3-fold excess of dry dichloromethane (Roth) was added to precipitate Na[dca], followed by subsequent filtration. Finally, the liquid was again dried under vacuum and stored over molecular sieves.

The synthesis of the IL was performed under nitrogen atmosphere. [emim]Cl and Na[dca] were purchased from Io-Li-Tec GmbH & Co. KG, [emim]Cl was purified twice by recrystallization (methanol/acetone = 1:10) and obtained as an almost white solid. The [emim][dca] was synthesized according to an anion metathesis procedure described in the literature.<sup>20</sup> In addition, the IL was treated with activated charcoal and dry dichloromethane, and dried under vacuum as described above. It was obtained as a slightly yellow liquid. The water content of the IL, determined by Karl Fisher titration,<sup>21</sup> was determined to be 370 mM.

**Instrumentation and Measurements.** Karl Fisher titrations were done on a Model 756 KF Coulometer (Metrohm). Elemental analyses (Euro EA 3000 (Euro Vector) and EA 1108 (Carlo Erba)) and NMR spectroscopy (Bruker Avance Model DRX 400 WB FT spectrometer) were used for chemical analysis and compound characterization, respectively. The UV–vis spectra were recorded on a Varian Cary 1G spectrophotometer equipped with a thermostatted cell holder and also on a Fluorolog 3 Horiba Jobin–Yvon spectrofluorometer.

**Thermodynamic Studies on the Reaction.** In a typical experiment, deoxygenated [emim][dca] was saturated with NO in a gas-tight syringe.<sup>22,23</sup> The NO solution was then mixed with a deoxygenated Fe(II) ionic liquid solution in a tandem cuvette in a 1:1 volume ratio. The equilibrium constant  $K_{\text{eq}}$  was determined via absorbance change measurements at 460 nm and ambient pressure at different temperatures in tandem cuvette experiments. The pressure dependence of the equilibrium constant  $K_{\text{eq}}$  was measured between 5 and 150 MPa on a Shimadzu Model UV-2101 PC UV–vis spectrophotometer equipped with a custom-built high-pressure cell and the use of a quartz pill-box cuvette.<sup>24</sup> The high-pressure pump was purchased from Nova Swiss<sup>25</sup> and enabled measurements in the selected pressure range. The measurements were carried out at 6 °C to slow the decomposition of the nitrosyl complex during the time of the experiment. In all experiments, pressure cycles were performed to ensure that spectra collected while the pressure increased coincided exactly with spectra recorded during the subsequent decrease in pressure.

**Kinetic Studies on the Reaction via Laser Flash Photolysis.** Solutions were prepared as mentioned above, but were mixed in gas-tight syringes

and then transferred to a cuvette. Laser flash photolysis kinetic studies were carried out with the use of the Model LKS.60 spectrometer from Applied Photophysics for detection and a Nd:YAG laser (SURLITE I-10 Continuum) pump source operating at the second ( $\lambda_{\text{exc}} = 532 \text{ nm}$ ) harmonic (245-mJ pulses with a pulse width of  $\sim 7 \text{ ns}$ ). Spectral changes at 460 nm were monitored using a 100 W xenon arc lamp, monochromator, and photomultiplier tube (Model PMT-1P22). The absorbance reading was balanced to zero before the flash, data were recorded on a digital storage oscilloscope (Model DSO HP 54522A), and then transferred to a computer for subsequent analysis. Gas-tight quartz cuvettes and a pill-box cell combined with high-pressure equipment<sup>15,24</sup> were used under ambient and high-pressure (between 5 and 150 MPa) conditions, respectively. Rate constants reported are mean values of at least 60 kinetic runs, and the quoted uncertainties are based on standard deviations. In all experiments, pressure cycles were performed to ensure that kinetic data collected during the increase in pressure coincided exactly with kinetic data recorded during the subsequent decrease in pressure.

**Mössbauer Spectroscopy.** A solution of 0.2 M  $\text{FeCl}_2$  in deoxygenated  $[\text{emim}][\text{dca}]$  was saturated with NO at 298 K in a gas-tight syringe and then rapidly placed into the Teflon container positioned in the brass inlet. The solution was frozen by immersing the sample into liquid nitrogen before decomposition of the nitrosyl complex could start. Afterward, the samples were mounted into the Mössbauer probe head that was placed into the precooled cryostat at 77 K.

<sup>57</sup>Fe Mössbauer spectra were recorded on a WissEl Mössbauer spectrometer (Model MRG-500) at 77 K in the constant acceleration mode. <sup>57</sup>Co/Rh was used as the radiation source. WinNormos for Igor Pro software was used for the quantitative evaluation of the spectral parameters (least-squares fitting to Lorentzian peaks). The minimum experimental line widths were  $0.20 \text{ mm s}^{-1}$ . The temperature of the samples was controlled by an MBBC-HE0106 Mössbauer He/N<sub>2</sub> cryostat within an accuracy of  $\pm 0.3 \text{ K}$ . Isomer shifts were determined relative to  $\alpha$ -iron at 298 K. Experimentally obtained spectra were simulated with MFIT Simulation Program, Version 1.1, E. Bill, MPI for Bioinorganic Chemistry, Mülheim an der Ruhr, Germany.

**EPR Spectroscopy.** Perpendicular-mode EPR spectra were recorded on a JEOL continuous-wave spectrometer (Model JES-FA200) that was equipped with an X-band Gunn diode oscillator, a cylindrical mode cavity, and a liquid helium cryostat. The EPR measurements were performed in quartz tubes at 20 K. Data analyses were performed using the Jes-Fa Series software package.

A solution of 1.2 mM  $\text{FeCl}_2$  in deoxygenated  $[\text{emim}][\text{dca}]$  was saturated with NO at 298 K in a gas-tight syringe and then rapidly filled into the EPR quartz tube. The solution was frozen by immersing the sample into liquid nitrogen before the decomposition of the nitrosyl complex could start. The samples were afterward mounted into the EPR probe head that was placed into the precooled cryostat at 20 K. In addition, the spectra of a 1.2 mM  $\text{FeCl}_3$  solution, a 1.2 mM  $\text{FeCl}_2$  solution before saturation with NO, and a saturated NO solution in deoxygenated  $[\text{emim}][\text{dca}]$  were also recorded in the same manner as described above, to enable better evaluation of the spectrum of the nitrosyl complex.

**IR Spectroscopy.** IR spectra of liquid samples were recorded with the use of a two-mirror ATR cell on an ATI Mattson FTIR Infinity spectrometer. The reflection instrument utilizes a germanium crystal as an internal reflection plate with a size of  $50 \text{ mm} \times 20 \text{ mm} \times 2 \text{ mm}$  and a  $45^\circ$  angle of incidence. Furthermore, IR spectra of liquid samples were also recorded with a  $\text{CaF}_2$  cuvette (0.05 mm). The pure IL, solutions of 0.05 and 0.5 M  $\text{FeCl}_2$  in deoxygenated  $[\text{emim}][\text{dca}]$ , and a solution of 0.2 M  $\text{FeCl}_2$  in deoxygenated  $[\text{emim}][\text{dca}]$  saturated with NO at 298 K were studied using both IR techniques. The IR spectrum of the isolated complex  $[\text{Fe}(\text{dca})_3\text{Cl}][\text{emim}]_2$  was obtained from a KBr disk. For every studied species, independent measurements of 300 scans (ATR-IR) or 50 scans ( $\text{CaF}_2$  cuvette or KBr disk) were performed under an inert gas atmosphere.

**Table 2. Crystallographic Data for  $[\text{Fe}(\text{dca})_3\text{Cl}][\text{emim}]_2 \cdot x$  Collected at 150 K<sup>a</sup>**

parameter	value/remark
empirical formula	$\text{C}_{18}\text{H}_{22}\text{ClFeN}_{13}$
<i>M</i>	$511.79 \text{ g mol}^{-1}$
system	monoclinic
space group	$P2_1/c$
<i>a</i>	$17.674(2) \text{ \AA}$
<i>b</i>	$11.645(2) \text{ \AA}$
<i>c</i>	$12.002(2) \text{ \AA}$
<i>V</i>	$2370.4(5) \text{ \AA}^3$
$\alpha$	$90^\circ$
$\beta$	$106.334(2)^\circ$
$\gamma$	$90^\circ$
<i>Z</i>	4
$\rho_{\text{calcd}}$	$1.434 \text{ g cm}^{-3}$
$\mu(\text{Mo K}\alpha)$	$0.784 \text{ mm}^{-1}$
<i>F</i> (000)	1056
$\theta$ range	$2.97^\circ\text{--}27.87^\circ$
reflections collected	24625
independent reflections, $R_{\text{int}}$	5637, 0.0311
independent reflections with $I > 2\sigma(I)$	4761
parameters refined	302
$R_1[F^2 > 2\sigma(F)^2]$	0.0305
$wR_2(F^2)$	0.0784

<sup>a</sup> Estimated standard deviations in the last significant digits are given in parentheses.

**X-ray Crystal Structure Determination.**  $[\text{Fe}(\text{dca})_3\text{Cl}][\text{emim}]_2 \cdot x$  was synthesized from  $\text{FeCl}_2$  (200 mg, 1.58 mmol) dissolved in  $[\text{emim}][\text{dca}]$  by stirring under vacuum at  $40^\circ\text{C}$  overnight. The clear solution was placed in the refrigerator ( $4^\circ\text{C}$ ), and, after two days, colorless crystals formed that were suitable for X-ray analysis. Molecular weight:  $511.76 \text{ g/mol}$ . Elemental Analysis: Calculated (%) for  $\text{C}_{18}\text{H}_{22}\text{N}_{13}\text{ClFe}$ : C, 42.25; H, 4.33; N, 35.58; Found: C, 41.23; H, 4.06; N, 36.14. A block-shaped crystal with a size of approximately  $0.20 \text{ mm} \times 0.08 \text{ mm} \times 0.06 \text{ mm}$  was covered with protective perfluoropolyalkylether oil and transferred into the cold  $\text{N}_2$  gas stream of the diffractometer. Intensity data of the crystal were collected at  $150(2) \text{ K}$  on a Bruker Kappa APEX 2 I $\mu$ S Duo diffractometer, using focusing QUAZAR Montel optics (Mo  $\text{K}\alpha$  radiation,  $\lambda = 0.71073 \text{ \AA}$ ). Data were corrected for Lorentz and polarization effects, and semiempirical absorption corrections were performed on the basis of multiple scans using SADABS.<sup>26</sup> The structure was solved by direct methods and refined by full-matrix least-squares procedures on  $F^2$ , using SHELXTL NT 6.12.<sup>27</sup> All non-hydrogen atoms were refined with anisotropic displacement parameters. The hydrogen atoms were placed in positions of optimized geometry, their isotropic displacement parameters were tied to those of the corresponding carrier atoms by a factor of 1.2 or 1.5. Cambridge Crystallographic Data Centre structure CCDC-778167 contains the supplementary crystallographic data for this paper. These data can be obtained free of charge via the Internet at [http://www.ccdc.cam.ac.uk/data\\_request/cif](http://www.ccdc.cam.ac.uk/data_request/cif) (or from Cambridge Crystallographic Data Centre, 12 Union Road, Cambridge, CB2 1EZ, UK (fax: +44-1223-336-033; E-mail: [deposit@ccdc.cam.ac.uk](mailto:deposit@ccdc.cam.ac.uk))).

## RESULTS AND DISCUSSION

**The Nature of the Fe(II) Complex in Solution.** It is well-known that, upon dissolving  $\text{FeCl}_2$  in water,  $[\text{Fe}(\text{H}_2\text{O})_6]^{2+}$  is formed in a weakly acidic solution. Via a subsequent reversible

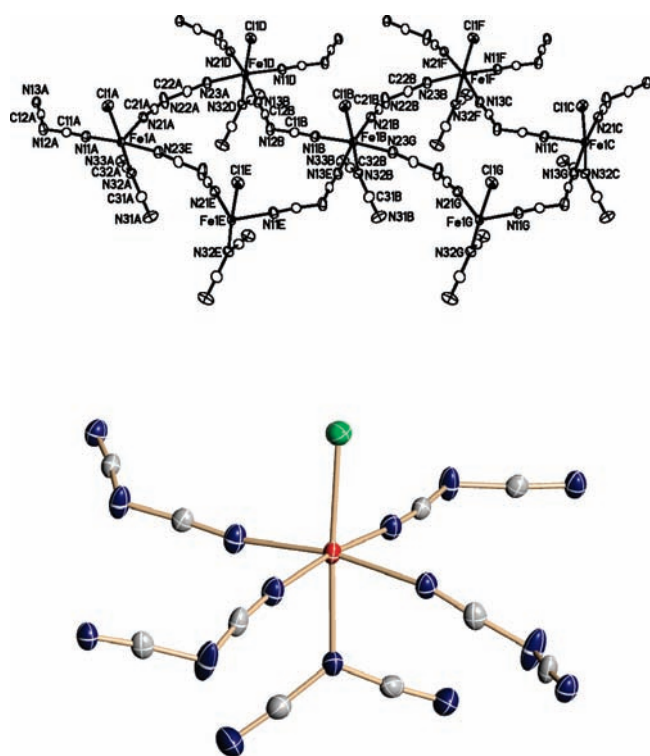


**Figure 1.** Structural information on the polymeric Fe(II) complex isolated from [emim][dca] (top) and the monomeric species proposed to be present in the IL solution (bottom, 50% probability ellipsoids (red denotes Fe atoms, green denotes Cl atoms, blue denotes N atoms, and gray denotes C)). See text for further information on bond parameters.

reaction with NO, one of the aqua ligands is displaced by NO to form the characteristic green-brown  $[\text{Fe}(\text{H}_2\text{O})_5\text{NO}]^{2+}$  complex. The transfer of this reaction from an aqueous to an IL medium brings about questions concerning the structure of the ferrous reactant and product species, as the situation becomes significantly more complicated in an IL. There are three potential ligands present in the IL, viz, (1) chloride ions from  $\text{FeCl}_2$  that was used as a Fe(II) source; (2) water molecules present in the very hygroscopic IL, despite thorough drying; and (3) the [dca] anions of the IL itself, which are known for their coordination ability.<sup>28,29</sup> The crystal structure of the ferrous complex isolated from the IL helped to clarify the situation. Upon dissolving  $\text{FeCl}_2$  in [emim][dca], colorless crystals precipitated at low temperature (4 °C) and revealed a coordination polymer of Fe(II) complexes. Polymeric dicyanamide-bridged iron(II) complexes are known from the literature,<sup>30–33</sup> but, as far as we know, there is no evidence for such complexes obtained directly from the IL medium. The crystal structure was resolved at 150 K, the crystal system belongs to the monoclinic system, space group  $P2_1/c$  ( $Z = 4$ ) (see Table 2 for further crystallographic data).

Every metal center in the cluster exhibits a distorted octahedral coordination sphere, formed by one Cl and five N atoms, four of which are from [dca] ligands coordinated via cyano N atoms and the fifth one is from a [dca] ligand coordinated via the amide N atom (see Figure 1). As a result of a high electron density on the terminal N atoms of [dca], coordination through these donors is much more probable than via the amide nitrogen,<sup>29</sup> although molecular structures for the latter case are also known in the literature.<sup>34</sup> It is remarkable that no water molecule is included in

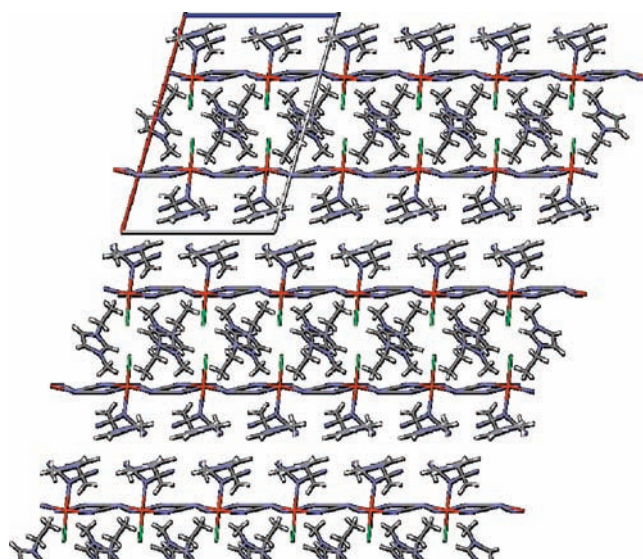


**Figure 2.** Projection of the molecular structure along the *b*-axis.

the structure, which suggests that the current water content does not affect the studied reaction, under the employed conditions. However, we assume that the polymer found in the solid state does not exist as such in solution, and, instead, monomeric  $[\text{Fe}(\text{dca})_5\text{Cl}]^{4-}$  units are present, as shown in Figure 1 (see further discussion).

The Fe–N distances for the cyano-nitrogen-coordinated [dca] ligands in the equatorial plane are slightly different and vary between 2.145(2) Å and 2.162(2) Å. Similar values are also known from the literature for polymeric compounds with bridging  $\mu_{1,5}$ -dca anions.<sup>35</sup> They are typical for a high-spin Fe(II) complex.<sup>30,36</sup> The results from Mössbauer spectroscopy given below also confirm that the starting Fe(II) complex is in the high-spin state. The Fe–N and Fe–Cl distances for the two axial ligands are 2.281(2) Å and 2.4218(6) Å, respectively. All N–Fe–N angles are  $<90^\circ$  and all Cl–Fe–N angles are  $>90^\circ$ , instead of  $90^\circ$  for a regular octahedron. The angles Cl–Fe–N23 and N32–Fe–N23 show the largest values ( $96.39(4)^\circ$  and  $87.41(5)^\circ$ , respectively), since the N32–Fe and Cl–Fe bonds are slightly bent toward the N11-coordinated [dca]. The distances found for the N–C (mean value: 1.15 Å) and C–N (mean value: 1.31 Å) bonds and the angles C–N–C ( $120^\circ$  or  $117^\circ$ ) and N–C–N ( $173^\circ$  or  $175^\circ$ ) of the equatorial and axial [dca] ligands show good agreement with values given in the literature.<sup>29</sup> These parameters confirm a distinct deviation from linearity and a marked participation of strongly delocalized  $\pi$ -bonds. If one brings the four donor-N atoms of the equatorial coordinated [dca] ligands in one plane, the metal center and the chloride ligand are positioned on one side of it, with out-of-plane distances for Fe of 0.163 Å and Cl of 2.583 Å, and the axial-coordinated [dca] ligand on the other side, with an out-of-plane distance for N32 of 2.116 Å. Two of the equatorially linked [dca] (via N11 and N13) lie on the same side as the iron center above the plane, and two further ligands (via N23 and N21) are on the side of the axial [dca] beneath it.

The dicyanamide ion shows a considerable tendency to function as a bidentate ligand and forms strong bridges between transition-metal atoms, sometimes yielding stable anionic coordination polymers.<sup>29,33</sup> Also, in the present crystal structure, each Fe cation is connected via  $\mu$ -1,5-dicyanamide bridging

Table 3. IR Bands of Dicyanamide in the High-Frequency Region Obtained from ATR–FTIR Measurements or KBr Disc

compound	IR Bands (cm <sup>-1</sup> )			reference
	$\nu_{as}(\text{C}\equiv\text{N}) + \nu_s(\text{C}\equiv\text{N})$	$\nu_{as}(\text{C}\equiv\text{N})$	$\nu_s(\text{C}\equiv\text{N})$	
Na[N(CN) <sub>2</sub> ]	2287	2229	2181	43c
[PPh <sub>4</sub> ][N(CN) <sub>2</sub> ]	2227	2188	2130	44
[emim][dca]	2228	2192	2130	this work
[Fe(dca) <sub>5</sub> Cl] <sup>4+</sup> complex, 0.5 M <sup>a</sup>	2257		2150	this work
[Fe(dca) <sub>5</sub> Cl] <sup>4+</sup> complex, 0.5 M <sup>b</sup>	2261	2211	2156	this work
[Fe(dca) <sub>5</sub> Cl] <sup>4+</sup> complex, 0.05 M <sup>b</sup>	2260	2204	2154	this work
Cp(dppe)FeN(CN) <sub>2</sub>	2266	2224	2158	43c
{Fe(bztpen)[N(CN) <sub>2</sub> ]}PF <sub>6</sub> ·CH <sub>3</sub> OH	2160	2220	2259	43b
Cp(PPh <sub>3</sub> ) <sub>2</sub> RuN(CN) <sub>2</sub>	2270	2229	2164	43c
[Fe(dca) <sub>3</sub> Cl][emim] <sub>2</sub>	2291/2274	2242/2228	2173/2160	this work
[Fe(dca) <sub>2</sub> (MeOH) <sub>2</sub> ]	2306/2274	2254	2178/2154	43e
[Mn(dca) <sub>2</sub> (py) <sub>2</sub> ]	2295	2234	2167	45
[Cu(dca) <sub>2</sub> (pz) <sub>2</sub> ]	2296	2240	2182	46

<sup>a</sup> Original spectrum; <sup>b</sup> Corrected spectrum

equatorial ligands with four neighboring metal cations. The Fe–Fe distances with 8.308 Å to the metal centers on the same side of the plane formed by four equatorial donor-N atoms, or 8.414 Å to the metal centers on the other side of this plane, are in good agreement with values for similar structural elements found in the literature.<sup>30</sup> This polymeric arrangement results in a two-dimensional structure of high symmetry. Projection of the molecular structure along the *b*-axis shows that axial ligands are parallel and coincide (see Figure 2), the counter-clockwise rotation of the structure at 45° results in only every second axial ligand parallel to each other and coinciding (see Figure S1 in the Supporting Information), the rotation of the structure 45° further makes the axial ligands coincide completely again (see Figure S2 in the Supporting Information). The resulting view is the projection along the *c*-axis, which displays the Cl–Fe-bonds bending toward the neighboring metal complex units. Over every layer lies another infinite sheet, with chloro ligands of two layers facing each other. These “sandwich” units repeat themselves, providing a three-dimensional network.

Amide-nitrogen coordinated [dca] ligands point outside of the “sandwich”, facing the axial linked [dca] from the neighbor “sandwich” and lying shifted by one to each other (see Figure 2). Between the axial [dca] ligands of directly bridged iron centers, [emim] rings lie in parallel planes. The rings, which belong to the neighboring layers lie directly above each other, with distances of 3.480 Å. Similar values are known from the literature, where aromatic ligands of adjoining chains form  $\pi$  bonding stacks.<sup>35</sup> Found distances are pointing to  $\pi^+ - \pi^+$  interactions between the aromatic systems of the imidazolium cations, and these are somewhat shorter than the  $\pi^+ - \pi$  distances found in the literature.<sup>37</sup> The rings are arranged such that H(2) of the [emim] cation points toward the N atom of the axial [dca] ligand from the next row in the same layer; the H–N distance is 2.407 Å, which lies between values of 2.52 Å<sup>38</sup> and 2.24 Å,<sup>39</sup> given for the equally close interionic C(2)–H···N(cyano) contact, which suggests the presence of a hydrogen bond.

The axial-linked chloro ligands point toward each other to form a type of “tunnel”, which hosts further [emim] rings (see Figure 2). These lie in planes parallel to each other, with every second ring twisted by 180°, resulting in the first and third ring coinciding. The distances between the planes are 3.428 Å,

pointing to  $\pi^+ - \pi^+$  interactions between the aromatic systems of the imidazolium cations as described above. The distance between the chloro-ligand and the H(2) of the [emim] cation is 2.871 Å, which is shorter than the sum of their van der Waals radii: Cl (1.8 Å) + H (1.4 Å) = 3.2 Å.<sup>40</sup> This is consistent with the intermolecular weak C–H···Cl–M nonclassical hydrogen bonds known from the literature.<sup>41</sup>

As mentioned above, we have good reason to believe that it is the monomeric [Fe(dca)<sub>5</sub>Cl]<sup>4+</sup> complex that undergoes the reaction with NO in the IL medium, despite the tendency of dicyanamide as a bi/tridentate ligand to form strong bridges between transition-metal centers, as discussed above. This is based on results obtained from IR measurements. Köhler et al.<sup>42</sup> reported that dicyanamide complexes of d-metals show almost the same number of IR bands as ionic alkali-metal dicyanamide species in the range of 2000–2400 cm<sup>-1</sup>, and that the shift in these bands point to the formation of dative bonds in such complexes. Characteristic stretching vibration bands of terminal dicyanamide ligands in mononuclear complexes are shifted to lower frequencies due to the  $\sigma$  donation from the ligand to the metal center upon coordination. The  $\nu(\text{N}(\text{CN})_2)$  values of the dicyanamide bridged complexes are shifted to higher frequencies, because of the integrated electronic effect of  $\sigma$  donation from the bridging ligand to the organometallic centers, as well as  $\pi$  back-donation from the organometallic center to the ligand. During the last three decades, many experimental results were reported that confirmed this suggestion.<sup>43</sup>

Therefore, we performed detailed IR measurements on the relevant iron(II) compounds in [emim][dca] solution. First, we applied ATR–IR spectroscopy, since one of the advantages of this method is the limited path length into the liquid sample, which avoids the problem of strong attenuation of the IR signal in strongly absorbing media, such as the studied IL.

In order to gain information on the monomeric vs polymeric structure of the studied species, we selected two crucial concentrations, viz, 0.5 M Fe(II), which is the concentration of the solution from which the polymeric compound precipitated, and 0.05 M Fe(II), which is the highest concentration used in the thermodynamic and kinetic studies. The observed stretching frequencies for dicyanamide in the high-frequency region are

Table 4. IR Bands of Dicyanamide in the High-Frequency Region Measured by FTIR Spectroscopy in a CaF<sub>2</sub> Cuvette (0.05 mm)

compound	IR Bands (cm <sup>-1</sup> )			reference
	$\nu_{\text{as}}(\text{C}\equiv\text{N}) + \nu_{\text{s}}(\text{C}\equiv\text{N})$	$\nu_{\text{as}}(\text{C}\equiv\text{N})$	$\nu_{\text{s}}(\text{C}\equiv\text{N})$	
[PPh <sub>4</sub> ][N(CN) <sub>2</sub> ]	2227	2188	2130	44
[emim][dca]	2220	2189	2149	this work
Na[N(CN) <sub>2</sub> ]	2287	2229	2181	43c
[Fe(dca) <sub>5</sub> Cl] <sup>4-</sup> complex, 0.5 M		2215	2163	this work
[Fe(dca) <sub>5</sub> Cl] <sup>4-</sup> complex, 0.2 M		2207	2168	this work

summarized in Table 3 and compared with the data reported in the literature. The pure [emim][dca] liquid shows bands that are more similar to those found for [PPh<sub>4</sub>][N(CN)<sub>2</sub>]<sup>44</sup> than for Na[N(CN)<sub>2</sub>],<sup>43c</sup> probably because of the fact that bulky organic cations prevent the strong interactions with the anion effective in Na[N(CN)<sub>2</sub>].

The spectrum of 0.05 M Fe(II) in [emim][dca] did not reveal much information concerning the nature of the dicyanamide complex, as the strong signals coming from the solvent itself covered the potential bands of the dicyanamide complex. However, in the case of the 0.5 M Fe(II) solution, the signals of the dicyanamide complex started to appear, along with bands of the IL and clearly showed a shift toward lower frequencies, relative to that for Na[N(CN)<sub>2</sub>] (see Table 3 and Figure S3 in the Supporting Information).

To eliminate the effect of the solvent, the spectrum of [emim][dca] was subtracted from the spectra of the 0.05 and 0.5 M Fe(II) solutions. The corrected spectra clearly show that the characteristic  $\nu(\text{N}(\text{CN})_2)$  bands are notably shifted to lower frequencies, compared to that of Na[N(CN)<sub>2</sub>] (see Table 3). Based on the literature information described above, this observation suggests the presence of monomeric species in the studied solutions. Table 3 also includes some examples of monomeric iron and ruthenium complexes that exhibit very similar  $\nu(\text{N}(\text{CN})_2)$  values, confirming the monomeric nature of the studied iron(II) dicyanamide complex in the IL. Moreover, the very similar  $\nu(\text{N}(\text{CN})_2)$  values found for both Fe(II) concentrations underline the existence of monomeric species, even in the 0.5 M Fe(II) solution from which the polymeric crystals were isolated.

To verify the obtained results and to test the applicability of another IR technique for ILs, we performed FTIR measurements in a CaF<sub>2</sub> cuvette with a particularly short optical path length to minimize the attenuation of the strong absorbing solvent. The results are in very good agreement with those obtained by ATR-FTIR, and the characteristic  $\nu(\text{N}(\text{CN})_2)$  bands in the high-frequency region are reported in Table 4.

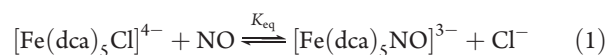
The bands for the pure IL again lie closer to those found for [PPh<sub>4</sub>][N(CN)<sub>2</sub>] than to those observed for Na[N(CN)<sub>2</sub>]. In the case of the lower Fe(II) concentration (0.05 M), these bands cover the signals coming from the dicyanamide complex. For higher Fe(II) concentrations (0.2 and 0.5 M), additional bands with similar values appear, which are shifted to lower frequencies compared to  $\nu(\text{N}(\text{CN})_2)$  values for Na[N(CN)<sub>2</sub>] (see Table 4). Comparison of the data in Tables 3 and 4 reveals that the  $\nu(\text{N}(\text{CN})_2)$  values obtained with both methods nicely match each other and also those reported in the literature for other monomeric iron and ruthenium complexes. Hence, our results obtained with both IR methods indicate that, in the investigated IL, the monomeric iron(II) dicyanamide complex is present in

solution over the entire concentration range (up to 0.5 M). The fact that a polymeric complex was isolated from the highly concentrated Fe(II) solution must be related to the lower solubility of the polymer that favors crystallization over a longer period of time.

To complete our study, we performed IR measurements (KBr disk) on the [Fe(dca)<sub>3</sub>Cl][emim]<sub>2</sub> polymer that was isolated from the IL. The spectrum is presented in Figure S4 in the Supporting Information and shows characteristic stretching vibrations of the dicyanamide ligand in the range between 2100 cm<sup>-1</sup> and 2400 cm<sup>-1</sup>, which are in good agreement with data reported in the literature<sup>43e,45,46</sup> and are summarized in Table 3.

The large number of bands observed in the solid-state IR spectrum suggests a low-symmetry coordination environment around the Fe(II) metal center. The characteristic  $\nu(\text{N}(\text{CN})_2)$  values in the high-frequency region are partly shifted to higher frequencies, compared to those of Na[N(CN)<sub>2</sub>], and confirm the bridging state of the four dicyanamide ligands in the equatorial plane. The low-frequency shifted bands likely originate from the terminally bound axial dicyanamide ligand. Some examples of other [dca]-containing polymeric compounds are also listed in Table 3 and show similar values. Thus, the IR results strongly underline our expectation that the monomeric [Fe(dca)<sub>5</sub>Cl]<sup>4-</sup> complex is the one present in [emim][dca] solution and is responsible for the observed reaction with NO.

We further assume that one of the axial ligands is substituted by NO, most probably the chloro ligand, because the Fe–Cl bond is longer than the Fe–N bond for the *trans* [dca] ligand. The strong  $\sigma$ -donor effect of both terminal cyano groups through the coordinated amido-N atom results in a faster reaction in the IL, compared to an aqueous medium, which is accompanied by a mechanistic shift from I<sub>d</sub> to D, as discussed in detail below. Based on this information, the overall reaction that occurs in the IL medium can be expressed by reaction 1 (see further discussion).



**Thermodynamic Study.** The UV–vis spectrum of [Fe(dca)<sub>5</sub>Cl]<sup>4-</sup> measured in [emim][dca] exhibits no absorption band between 300 nm and 800 nm, as can be seen from Figure 3. Measurements below 300 nm were not possible in the IL, because of the spectral properties of the selected IL. Despite all the cleaning procedures described above, [emim][dca] remains slightly yellow and shows an absorbance of 1.0 at ~320 nm (see Figure S5 in the Supporting Information). As can be seen from Figure 3, exposure of a degassed solution of [Fe(dca)<sub>5</sub>Cl]<sup>4-</sup> to excess NO leads to a significant increase in absorbance, resulting

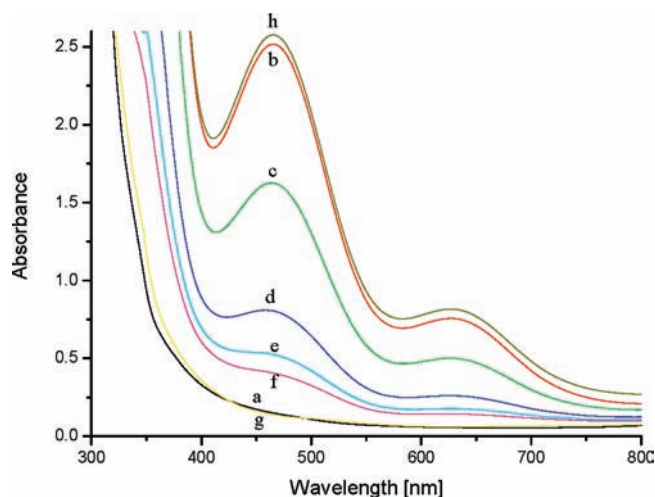


**Figure 3.** Absorption spectral changes recorded for the reaction of  $9 \times 10^{-3}$  M  $[\text{Fe}(\text{dca})_5\text{Cl}]^{4-}$  with NO in  $[\text{emim}][\text{dca}]$  at room temperature. Curves:  $[\text{Fe}(\text{dca})_5\text{Cl}]^{4-}$  solution (trace a);  $[\text{Fe}(\text{dca})_5\text{Cl}]^{4-}$  solution saturated with NO (trace b); trace b + brief  $\text{N}_2$  (10 s) (trace c); trace b + brief  $\text{N}_2$  (30 s) (trace d); trace b + brief  $\text{N}_2$  (50 s) (trace e); trace b + brief  $\text{N}_2$  (70 s) (trace f); trace b + brief  $\text{N}_2$  (10 min) (trace g); and trace g + brief NO (3 min) (trace h).

in band maxima at 465 and 630 nm. These are shifted to longer wavelengths, compared to those found in water used as a solvent (viz, 451 and 585 nm).<sup>18</sup> In the selected IL the formation of the nitrosyl complex is completely reversible, which was tested through alternate bubbling of NO and  $\text{N}_2$  through the Fe(II) solution (see Figure 3), indicating that the reversible nature of the equilibrium described in reaction 1 must be valid under the selected conditions.

Measurements on the thermodynamic behavior of reaction 1, as a function of temperature and pressure, should enable determination of the standard reaction parameters  $\Delta H^\circ$ ,  $\Delta S^\circ$ , and  $\Delta V^\circ$ , respectively.<sup>47</sup> First, we determined the overall equilibrium constant at room temperature by performing a spectrophotometric titration for reaction 1 by following the change in absorbance ( $\Delta\text{Abs}$ ) at 460 nm for mixing various concentrations of Fe(II) with NO, as shown in Figure S6 in the Supporting Information. The value of  $K_{\text{eq}}$  was calculated according to eq 2, where  $A_0$  and  $A_\infty$  represent the absorbance of  $[\text{Fe}(\text{dca})_5\text{Cl}]^{4-}$  and  $[\text{Fe}(\text{dca})_5\text{NO}]^{3-}$ , respectively, and  $A_x$  is the absorbance at any Fe(II) concentration. From the data in Figure S6 in the Supporting Information,  $K_{\text{eq}}$  was found to be equal to  $172 \pm 20 \text{ M}^{-1}$  at 25 °C, which is  $\sim 6$  times smaller than that found in water, viz,  $1150 \pm 50 \text{ M}^{-1}$ .<sup>18</sup> However, this difference is only a factor of 2, based on kinetic data for the reversible binding of NO in both solvents (see further discussion).

$$A_x = A_0 + \frac{(A_\infty - A_0)K_{\text{eq}}[\text{Fe}^{\text{II}}(\text{dca})_5\text{Cl}]^{4-}}{1 + K_{\text{eq}}[\text{Fe}^{\text{II}}(\text{dca})_5\text{Cl}]^{4-}} \quad (2)$$

To determine the standard reaction parameters  $\Delta H^\circ$  and  $\Delta S^\circ$ , the change in absorbance was followed in the temperature range of 20–40 °C. Figure 4 shows that the back reaction described by reaction 1 is favored upon increasing the temperature.  $K_{\text{eq}}$  values were calculated as a function of temperature, using the calibration curve in Figure S6 in the Supporting Information. A linear plot of  $\ln(K_{\text{eq}})$  vs  $1/T$  (see Figure S7 in the Supporting Information) enabled the determination of  $\Delta H^\circ = -37 \pm 1 \text{ kJ mol}^{-1}$  and

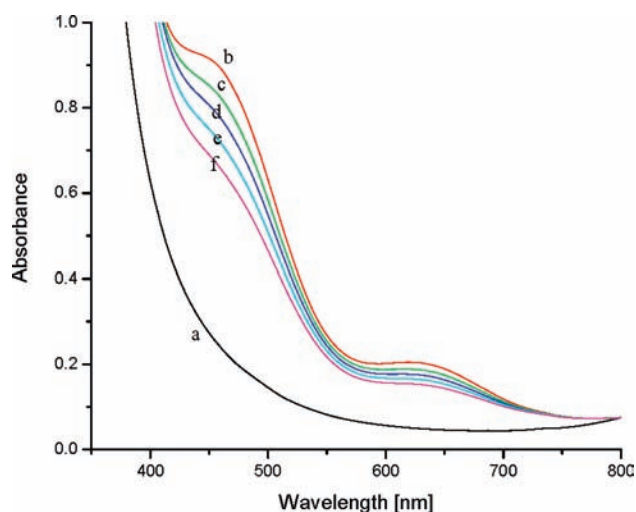


**Figure 4.** Temperature-dependent spectra recorded for the reaction of  $[\text{Fe}(\text{dca})_5\text{Cl}]^{4-}$  with NO in  $[\text{emim}][\text{dca}]$ . Curves:  $[\text{Fe}(\text{dca})_5\text{Cl}]^{4-}$  solution (trace a);  $[\text{Fe}(\text{dca})_5\text{NO}]^{3-}$  solution at 20 °C (trace b);  $[\text{Fe}(\text{dca})_5\text{NO}]^{3-}$  solution at 25 °C (trace c);  $[\text{Fe}(\text{dca})_5\text{NO}]^{3-}$  solution at 30 °C (trace d);  $[\text{Fe}(\text{dca})_5\text{NO}]^{3-}$  solution at 35 °C (trace e); and  $[\text{Fe}(\text{dca})_5\text{NO}]^{3-}$  solution at 40 °C (trace f). Experimental conditions:  $[\text{Fe}(\text{dca})_5\text{Cl}]^{4-} = 7.8 \text{ mM}$ ;  $[\text{NO}] = 7 \text{ mM}$ , ambient pressure.

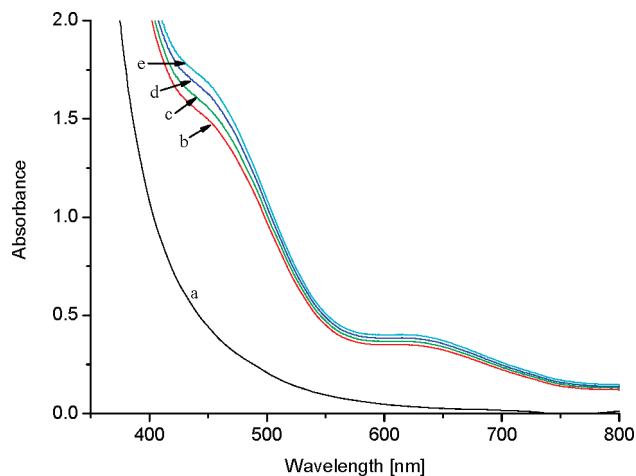


**Figure 5.** Pressure-dependent spectra recorded for the reaction of  $[\text{Fe}(\text{dca})_5\text{Cl}]^{4-}$  with NO in  $[\text{emim}][\text{dca}]$ . Curves:  $[\text{Fe}(\text{dca})_5\text{Cl}]^{4-}$  solution (trace a);  $[\text{Fe}(\text{dca})_5\text{NO}]^{3-}$  solution at 5 MPa (trace b);  $[\text{Fe}(\text{dca})_5\text{NO}]^{3-}$  solution at 50 MPa (trace c);  $[\text{Fe}(\text{dca})_5\text{NO}]^{3-}$  solution at 100 MPa (trace d); and  $[\text{Fe}(\text{dca})_5\text{NO}]^{3-}$  solution at 150 MPa (trace e). Experimental conditions:  $[\text{Fe}(\text{dca})_5\text{Cl}]^{4-} = 2 \text{ mM}$ ;  $[\text{NO}] = 7 \text{ mM}$ ,  $T = 6 \text{ }^\circ\text{C}$ .

$\Delta S^\circ = -81 \pm 4 \text{ J K}^{-1} \text{ mol}^{-1}$  from the slope and intercept, respectively, according to eq 3.

$$R \ln K_{\text{eq}} = -\frac{\Delta H^\circ}{T} + \Delta S^\circ \quad (3)$$

The pressure dependence of the equilibrium constant was studied at pressures up to 150 MPa and at a low temperature (6 °C), to prevent decomposition of the nitrosyl complex during the experiment. As shown in Figure 5, increasing the pressure favors formation of the nitrosyl complex. According to eq 4, a linear fit of  $\ln K_{\text{eq}}$  vs pressure (see Figure S8 in the Supporting

Scheme 1

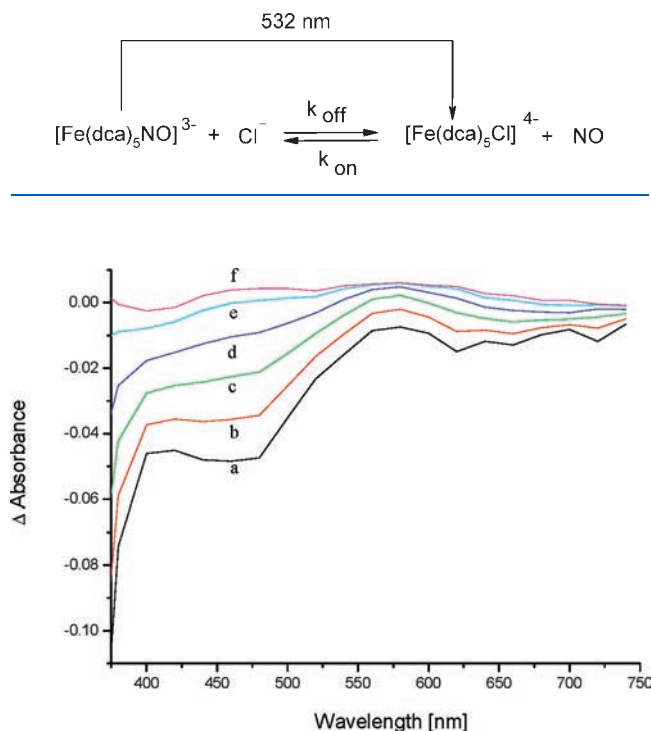


**Figure 6.** Transient absorption difference spectra for  $[\text{Fe}(\text{dca})_5\text{NO}]^{3-}$  after laser flash photolysis at 532 nm. Experimental conditions:  $[\text{Fe}(\text{dca})_5\text{Cl}]^{4-} = 15 \text{ mM}$ ,  $[\text{NO}] = 7 \text{ mM}$ , in  $[\text{emim}][\text{dca}]$  at 25 °C. Curves: after 0.135  $\mu\text{s}$  (trace a); after 0.455  $\mu\text{s}$  (trace b); after 0.915  $\mu\text{s}$  (trace c); after 1.61  $\mu\text{s}$  (trace d); after 3.01  $\mu\text{s}$  (trace e); and after 6.02  $\mu\text{s}$  (trace f).

Information) allows the determination of  $\Delta V^\circ = -7.5 \pm 0.2 \text{ cm}^3 \text{ mol}^{-1}$ .

$$\ln K_{\text{eq}} = -\frac{P}{RT} \Delta V^\circ \quad (4)$$

In summary, increased temperature and pressure have opposite effects on the binding of NO to  $[\text{Fe}(\text{dca})_5\text{Cl}]^{4-}$ . The temperature dependence clearly illustrates that the overall equilibrium in reaction 1 is shifted in the backward direction upon increasing the temperature, i.e., according to an exothermic reaction for which  $\Delta H^\circ$  has a negative value ( $-37 \pm 1 \text{ kJ mol}^{-1}$ ). In contrast, an increase in pressure leads to a shift in the forward direction of the equilibrium described in reaction 1 and favors the formation of the nitrosyl complex. This can be explained in terms of a decrease in the partial molar volume of the product, compared to the reactants, upon binding NO ( $\Delta V^\circ = -7.5 \pm 0.2 \text{ cm}^3 \text{ mol}^{-1}$ ).

**Flash-Photolysis Kinetics.** Rate constants for the reversible binding of NO to  $[\text{Fe}(\text{dca})_5\text{Cl}]^{4-}$  can be conveniently measured by flash photolysis, which can be employed to study the kinetics of reactions on a significantly faster time scale than stopped-flow techniques. Irradiation at 532 nm induces dissociation of the nitrosyl complex and rapid release of NO, followed by relaxation of the system back to the original equilibrium position (see Scheme 1).

As can be seen from Figure 6, 532-nm photolysis of  $[\text{Fe}(\text{dca})_5\text{NO}]^{3-}$  in  $[\text{emim}][\text{dca}]$  results in spectral changes that are described by prompt transient bleaching with the largest

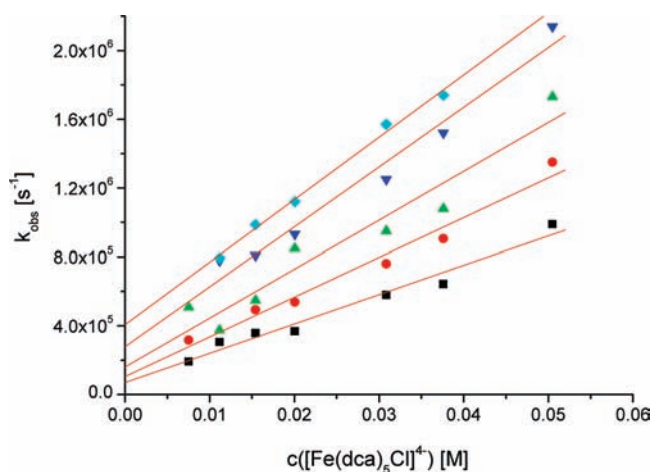


**Figure 7.** Plots of  $k_{\text{obs}}$  vs  $[\text{Fe}(\text{dca})_5\text{Cl}]^{4-}$  for the reaction of  $[\text{Fe}(\text{dca})_5\text{Cl}]^{4-}$  with NO over the temperature range of 20–40 °C, as measured by flash photolysis at 20 °C (squares), 25 °C (circles), 30 °C (triangles), 35 °C (stars), and 40 °C (diamonds). Experimental conditions:  $[\text{Fe}(\text{dca})_5\text{Cl}]^{4-} = 7.5\text{--}50.5 \text{ mM}$ ,  $[\text{NO}] = 7 \text{ mM}$ , in  $[\text{emim}][\text{dca}]$ ,  $\lambda_{\text{irr}} = 532 \text{ nm}$ ,  $\lambda_{\text{det}} = 460 \text{ nm}$ .

change in absorbance centered at 460 and 630 nm. This is consistent with the photolabilization of NO from  $[\text{Fe}(\text{dca})_5\text{NO}]^{3-}$  and formation of free NO and  $[\text{Fe}(\text{dca})_5\text{Cl}]^{4-}$ . After a delay of 6  $\mu\text{s}$ , the transient bleaching disappears and the spectrum returns to the baseline ascribed to the regeneration of the original nitrosyl complex. The application of 532-nm laser flash photolysis has the advantage that it prevents possible photodegradation of the IL that strongly absorbs below 350 nm.

The decay of the transient bleaching was followed using single-wavelength detection at 460 nm and could be analyzed as a single-exponential decay as shown in Figure S9 in the Supporting Information. As can be seen, the rebinding of NO to  $[\text{Fe}(\text{dca})_5\text{Cl}]^{4-}$  is completed within 4.8  $\mu\text{s}$  at  $[\text{Fe}(\text{dca})_5\text{Cl}]^{4-} = 0.05 \text{ M}$  and 25 °C, for which  $k_{\text{obs}} = 1.23 \times 10^6 \text{ s}^{-1}$ . The kinetic data obtained in this way turned out to be very reproducible.

The rate of the reaction approaching equilibrium with one of the components (in our case,  $[\text{Fe}(\text{dca})_5\text{Cl}]^{4-}$ ) in a large excess is expected to follow pseudo-first-order kinetics to give a rate constant  $k_{\text{obs}}$  expressed by eq 5:

$$k_{\text{obs}} = k_{\text{on}}[\text{Fe}(\text{dca})_5\text{Cl}]^{4-} + k_{\text{off}} \quad (5)$$

Accordingly, a plot of  $k_{\text{obs}}$  vs  $[\text{Fe}(\text{dca})_5\text{Cl}]^{4-}$  should be linear with a slope equal to  $k_{\text{on}}$  and an intercept equal to  $k_{\text{off}}$ . In the studied system, the equilibrium constant  $K_{\text{eq}}$  is sufficiently small that extrapolation to  $[\text{Fe}(\text{dca})_5\text{Cl}]^{4-} = 0$  gives a measurable intercept, i.e.,  $k_{\text{off}}$ . In agreement with eq 5, plots of  $k_{\text{obs}}$  vs  $[\text{Fe}(\text{dca})_5\text{Cl}]^{4-}$  are linear with nonzero intercepts as displayed in Figure 7 for the temperature range of 20–40 °C. The  $k_{\text{on}}$  and  $k_{\text{off}}$  values determined from these plots (see Table S5) at 25 °C were used to estimate the overall equilibrium constant  $K_{\text{eq}}$  for the reaction given in Scheme 1, which resulted in  $K_{\text{eq}} = k_{\text{on}}/k_{\text{off}} = 220 \pm 135 \text{ M}^{-1}$ . This value is in close agreement with the thermodynamically determined value, viz,  $K_{\text{eq}} = 172 \pm 20 \text{ M}^{-1}$ ; the large error limit on the kinetically determined value of  $K_{\text{eq}}$  is related to large errors involved in the determination of  $k_{\text{off}}$  via extrapolation of the kinetic data obtained in the flash-photolysis experiments.  $K_{\text{eq}}$  values also were calculated for the other temperatures, and they show a good correlation as well (see Table S5).



**Table 5.** Rate and Equilibrium Constants, as a Function of Temperature, for the Reversible Binding of NO to Fe(II) in [emim][dca] and Water as Solvents

temp (K)	[emim][dca]				H <sub>2</sub> O <sup>c</sup>		
	$k_{\text{on}}$ (M <sup>-1</sup> s <sup>-1</sup> )	$k_{\text{off}}$ (s <sup>-1</sup> )	$K_{\text{eq}}$ (M <sup>-1</sup> ) <sup>a</sup>	$K_{\text{eq}}$ (M <sup>-1</sup> ) <sup>b</sup>	$k_{\text{on}}$ (M <sup>-1</sup> s <sup>-1</sup> )	$k_{\text{off}}$ (s <sup>-1</sup> )	$K_{\text{eq}}$ (M <sup>-1</sup> ) <sup>a</sup>
293	$(1.7 \pm 0.1) \times 10^7$	$(7 \pm 4) \times 10^4$	$243 \pm 150$	$262 \pm 20$	$(1.06 \pm 0.10) \times 10^6$	$(2.38 \pm 0.22) \times 10^3$	$445 \pm 83$
298	$(2.3 \pm 0.2) \times 10^7$	$(1.0 \pm 0.6) \times 10^5$	$220 \pm 135$	$172 \pm 20$	$(1.42 \pm 0.04) \times 10^6$	$(3.2 \pm 0.7) \times 10^3$	$440 \pm 110$
303	$(2.8 \pm 0.4) \times 10^7$	$(1.6 \pm 1.0) \times 10^5$	$177 \pm 136$	$158 \pm 9$	$(1.86 \pm 0.03) \times 10^6$	$(4.42 \pm 0.59) \times 10^3$	$421 \pm 63$
308	$(3.5 \pm 0.3) \times 10^7$	$(2.8 \pm 0.9) \times 10^5$	$125 \pm 52$	$124 \pm 6$	$(2.31 \pm 0.05) \times 10^6$	$(7.05 \pm 0.90) \times 10^3$	$328 \pm 49$
313	$(3.6 \pm 0.2) \times 10^7$	$(4.1 \pm 0.4) \times 10^5$	$89 \pm 13$	$97 \pm 4$			

<sup>a</sup> Kinetically determined equilibrium constant:  $K_{\text{eq}} = k_{\text{on}}/k_{\text{off}}$ . <sup>b</sup> Thermodynamically measured equilibrium constant. <sup>c</sup> Data reported in the literature (ref 18).

**Table 6.** Activation and Reaction Parameters for the Reversible Formation of the Nitrosyl Complex in the Ionic Liquid [emim][dca] and Water as Solvents

	$\Delta H_{\text{on}}^{\ddagger}$ (kJ mol <sup>-1</sup> )	$\Delta S_{\text{on}}^{\ddagger}$ (J K <sup>-1</sup> mol <sup>-1</sup> )	$\Delta V_{\text{on}}^{\ddagger}$ (cm <sup>3</sup> mol <sup>-1</sup> )
IL	$27 \pm 4$	$-14 \pm 12$	$+14.3 \pm 0.5$
H <sub>2</sub> O	$37.1 \pm 0.5$	$-3 \pm 2$	$+6.1 \pm 0.4$
	$\Delta H_{\text{off}}^{\ddagger}$ (kJ mol <sup>-1</sup> )	$\Delta S_{\text{off}}^{\ddagger}$ (J K <sup>-1</sup> mol <sup>-1</sup> )	$\Delta V_{\text{off}}^{\ddagger}$ (cm <sup>3</sup> mol <sup>-1</sup> )
IL	$66 \pm 3$	$+73 \pm 9$	$+25 \pm 2$
H <sub>2</sub> O	$48 \pm 1$	$-15 \pm 5$	$+1.3 \pm 0.2$
	$\Delta H^{\circ}$ (kJ mol <sup>-1</sup> )	$\Delta S^{\circ}$ (J K <sup>-1</sup> mol <sup>-1</sup> )	$\Delta V^{\circ}$ (cm <sup>3</sup> mol <sup>-1</sup> )
IL	$-37 \pm 1$	$-81 \pm 4$	$-7.5 \pm 0.2$
H <sub>2</sub> O	$-11 \pm 2$	$+12 \pm 6$	$+4.8 \pm 0.6$

The temperature dependence of  $k_{\text{on}}$  and  $k_{\text{off}}$  (see Table 5) was used to construct linear Eyring plots (see Figure S10 in the Supporting Information), from which the activation parameters  $\Delta H^{\ddagger}$  and  $\Delta S^{\ddagger}$  were determined. They are summarized in Table 6 and compared with the data found in aqueous solution.<sup>18</sup> Since the  $k_{\text{off}}$  values are obtained by extrapolation of the  $k_{\text{obs}}$  vs  $[\text{Fe}(\text{dca})_5\text{Cl}]^{4-}$  plots, and the determination of  $\Delta S^{\ddagger}$  in principle involves an extrapolation to  $1/T = 0$ , it is reasonable to expect that the values of  $\Delta S^{\ddagger}$ , especially for the “off” reaction, will be subjected to large error limits. Thus, mechanistic conclusions based on the values reported for  $\Delta S^{\ddagger}$  are difficult to reach, especially when they are close to 0 (see Table 6).

A more reliable mechanistic discrimination parameter is the volume of activation (see eq 6, where  $k_i$  is the rate constant at a particular pressure)<sup>48</sup> derived from the effect of hydrostatic pressure  $P$  on the rate constant of the reaction.

$$\Delta V^{\ddagger} = -RT \left( \frac{d \ln k_i}{dP} \right)_T \quad (6)$$

The effect of pressure on the reaction of  $[\text{Fe}(\text{dca})_5\text{Cl}]^{4-}$  with NO was studied using a high-pressure flash-photolysis technique in the pressure range of 5–150 MPa. The results are presented in Figure 8.

From plots of  $k_{\text{obs}}$  vs  $[\text{Fe}(\text{dca})_5\text{Cl}]^{4-}$  at different pressures, values of  $k_{\text{on}}$  and  $k_{\text{off}}$  were determined (see Table S1 in the Supporting Information), and linear  $\ln(k_i)$  vs pressure plots (see Figure S11 in the Supporting Information) show that both rate constants decrease as the pressure increases, resulting in positive volumes of activation, viz,  $\Delta V_{\text{on}}^{\ddagger} = +14.3 \pm 0.5 \text{ cm}^3 \text{ mol}^{-1}$  and  $\Delta V_{\text{off}}^{\ddagger} = +25 \pm 2 \text{ cm}^3 \text{ mol}^{-1}$  for the “on” and “off”

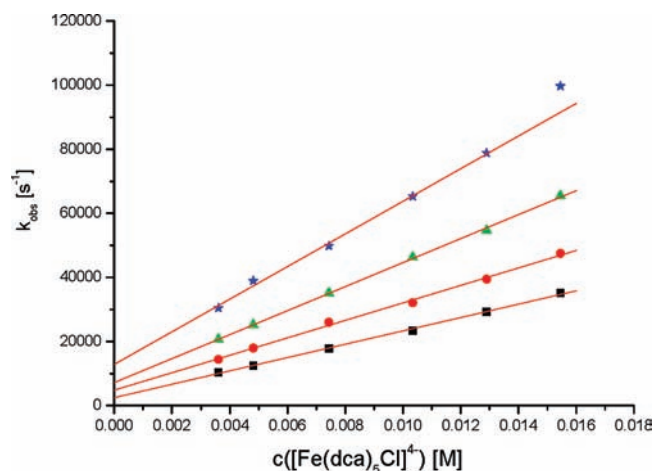


**Figure 8.** Plots of  $k_{\text{obs}}$  vs  $[\text{Fe}(\text{dca})_5\text{Cl}]^{4-}$  for the reaction of  $[\text{Fe}(\text{dca})_5\text{Cl}]^{4-}$  with NO over the pressure range of 5–150 MPa, as measured by flash photolysis at 150 MPa (squares), 100 MPa (circles), 50 MPa (triangles), and 5 MPa (stars). Experimental conditions:  $[\text{Fe}(\text{dca})_5\text{Cl}]^{4-} = 3.6\text{--}15.5 \text{ mM}$ ,  $[\text{NO}] = 7 \text{ mM}$ , in  $[\text{emim}][\text{dca}]$ ,  $\lambda_{\text{irr}} = 532 \text{ nm}$ ,  $\lambda_{\text{det}} = 460 \text{ nm}$ ,  $T = 279 \text{ K}$ .

reactions, respectively. The reaction volume ( $\Delta V^{\circ}$ ) for the overall equilibrium ( $\Delta V^{\circ} = \Delta V_{\text{on}}^{\ddagger} - \Delta V_{\text{off}}^{\ddagger}$ ) is  $-11 \pm 2 \text{ cm}^3 \text{ mol}^{-1}$ , indicating that there is an overall decrease in partial molar volume during the displacement of coordinated chloride by NO. This kinetically determined value is within the experimental error limits close to the thermodynamic value of  $-7.5 \pm 0.2 \text{ cm}^3 \text{ mol}^{-1}$ . A volume profile that has been constructed on the basis of the high-pressure kinetic data is given in Figure 9, which suggests that both the forward and back reactions in reaction 1 proceed according to a dissociative mechanism.

A comparison of the rate constants for the binding of NO to Fe(II) in  $[\text{emim}][\text{dca}]$  and water as solvent shows that both the “on” and “off” reactions are significantly faster in the IL than in water as a solvent (see Table 5). The  $k_{\text{on}}$  parameter increases by a factor of 16, whereas  $k_{\text{off}}$  increases by a factor of 31 at 25 °C upon going from an aqueous medium to the selected IL, such that the overall equilibrium constant decreases by a factor of 2, which is less than the factor of 6 based on the thermodynamic data reported above. In previous work performed in our group, we reported deceleration effects of ionic liquids for ligand substitution reactions of Pt(II) complexes<sup>9</sup> or for the reversible binding of NO to the monohydroxo ligated iron(III) porphyrin,  $(\text{TMPS})\text{Fe}^{\text{III}}(\text{OH})$ ,<sup>19</sup> caused by the polarity and nature of the IL. The principal difference

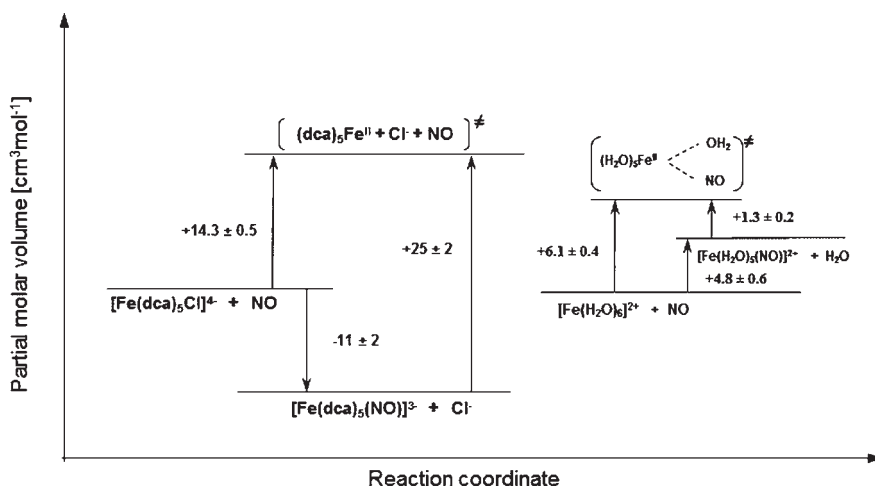


**Figure 9.** Volume profile for reaction 1, based on the determined volumes of activation (left), and by way of comparison the corresponding volume profile for the same reaction in aqueous medium (right) taken from ref 18.

in the present case results from the “non-innocent” influence of the IL as medium on the studied reaction. As explained above, the anion of the selected IL [dca] coordinates to the Fe(II) center and changes the nature of the reactant significantly and, with it, the course of the reaction compared to that in aqueous solution. The stronger acceleration of  $k_{\text{off}}$  than  $k_{\text{on}}$  in [emim][dca] is ascribed to the stronger labilization of coordinated NO in  $[\text{Fe}(\text{dca})_5\text{NO}]^{3-}$  than coordinated chloride in  $[\text{Fe}(\text{dca})_5\text{Cl}]^{4-}$  by the amide-N-coordinated [dca] ligand *trans* to NO and  $\text{Cl}^-$ , respectively.

The substitution of the chloro ligand is significantly influenced by the *trans* [dca] ligand. The strong  $\sigma$ -donor effect of both cyano groups on [dca] through the coordinated amido-N atom results in labilization of the Fe–Cl bond and acceleration of the reaction compared to that in aqueous solution, which is in agreement with a lower activation enthalpy ( $\Delta H^\ddagger$ ) value. The release of NO during the “off” reaction exhibits a much higher activation enthalpy than found for the “on” reaction, and is characterized by a more positive activation entropy, suggesting that solvent reorganization must play an important role in this process. As a result, the overall reaction enthalpy ( $\Delta H^\circ$ ) for the binding of NO exhibits a large negative value, i.e., the process is exothermic and  $K_{\text{eq}}$  decreases as the temperature increases.

A further consequence of the labilization effect of the *trans* [dca] ligand is the change from an  $\text{I}_\text{d}$  substitution mechanism observed in water to a limiting D mechanism in the IL, based on the large positive values of the activation volumes. This is clearly seen from a comparison of the volume profiles for the reversible binding of NO to Fe(II) in [emim][dca] and water as solvent given in Figure 9. The  $\Delta V^\ddagger$  values found for the “on” and “off” reactions in [emim][dca] confirm the dissociative pathway for both reactions and are close to the partial molar volumes for the chloride anion (calculated,  $14.95 \text{ cm}^3 \text{ mol}^{-1}$ ; measured,  $16.45 \text{ cm}^3 \text{ mol}^{-1}$ )<sup>49</sup> and NO molecule ( $27 \text{ cm}^3 \text{ mol}^{-1}$ ),<sup>50</sup> respectively. The overall negative reaction volume (obtained from kinetic as well as thermodynamic data in [emim][dca]) results from the displacement of chloride by NO in the coordination sphere of Fe(II) and is in good agreement with the negative value for  $\Delta S^\circ$  also found from both kinetic and thermodynamic data. The overall negative reaction volume found for [emim][dca], compared to the positive reaction volume found for water as a solvent (see Figure 9) can be considered in terms of the contribution of the very positive

activation volume found for the “off” reaction in [emim][dca]. The latter must be related to the strong labilization of coordinated NO by the amide-nitrogen in the *trans* position of  $[\text{Fe}(\text{dca})_5\text{NO}]^{3-}$ , as mentioned above.

**Stopped-Flow Kinetics.** Since the  $k_{\text{off}}$  values obtained from the  $[\text{Fe}(\text{dca})_5\text{Cl}]^{4-}$  concentration dependence of  $k_{\text{obs}}$  in the flash photolysis experiments are subjected to significant extrapolation errors (see Figures 7 and 8), we studied their reliability in a more direct way. As previously shown,<sup>18,51</sup> the most suitable method to measure  $k_{\text{off}}$  directly is to use an NO-trapping technique, combined with the stopped-flow method. In such a case, the nitrosyl product is treated with another complex that binds NO stronger and more rapidly than the system under investigation. When an excess of the trapping complex is employed, the release of NO from the nitrosyl complex becomes the rate-limiting step in the reaction sequence, and  $k_{\text{off}}$  can be determined directly from the observed kinetic trace, viz,  $k_{\text{obs}} = k_{\text{off}}$ . Such experiments were performed but turned out to be much more complicated than in aqueous solution, because of direct interaction of the IL with the trapping agent. These results will be reported in a subsequent communication from our laboratory.

**Spectroscopic Observations.** IR spectroscopy is considered to be a useful tool for the determination of the bonding mode and oxidation state of NO in metal-NO complexes.<sup>52</sup> According to the literature, free NO in solution does not exhibit any absorption bands that are readily detectable in the relevant window of the spectrum.<sup>53</sup> The ATR-IR measurements were successfully applied in the earlier study of the “brown ring” complex in aqueous solution;<sup>18</sup> however, in the case of [emim][dca] as a solvent, FTIR measurements using the  $\text{CaF}_2$  cuvette provided better results. Spectra of the starting Fe(II) solution and of the solution saturated with NO, were measured at room temperature and are reported in Figure 10. The formation of a single peak at  $1767 \text{ cm}^{-1}$  was clearly observed, indicating the formation of the  $[\text{Fe}(\text{dca})_5\text{NO}]^{3-}$  complex. Taking into account that, for a series of  $\text{Fe}^\text{II}(\text{L})\text{NO}$  complexes (L = polyaminocarboxylate) known to bind NO formally as  $\text{Fe}^\text{III}-\text{NO}^-$ ,<sup>54</sup> the observed wave numbers were found to be  $\sim 1777 \text{ cm}^{-1}$  (L =  $\text{edta}^{4-}$ ), the observed peak at  $1767 \text{ cm}^{-1}$  suggests that the product species can formally be written as  $[\text{Fe}^\text{III}(\text{dca})_5\text{NO}^-]^{3-}$ , indicating a pronounced electron donation from the metal to the ligand. Comparing the

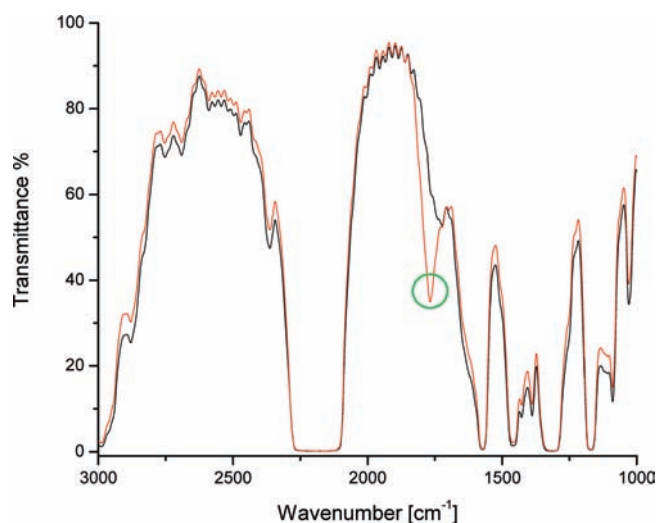


**Figure 10.** IR spectrum of the Fe(II) (black line) and nitrosylated Fe(II) solution (red line) in [emim][dca] at room temperature. Experimental conditions: 0.2 M Fe(II) solution saturated with NO at 298 K,  $\tilde{\nu} = 1767 \text{ cm}^{-1}$  (m, NO).

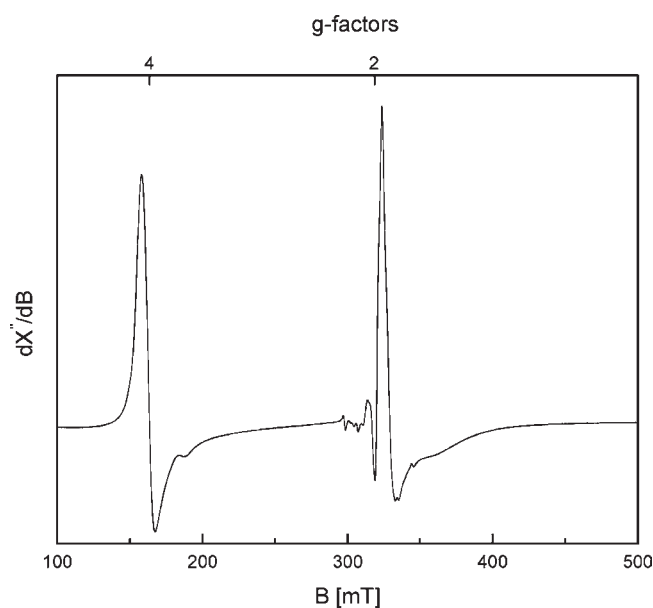


**Figure 11.** X-band EPR spectrum of the Fe(II) nitrosyl complex in [emim][dca]. Experimental conditions: 1.2 mM Fe(II) solution saturated with NO at 298 K, with a measuring temperature of 20 K, a microwave frequency of 8.9848 GHz, a power of 1 mW, and a modulation of 1.0 mT at 100 kHz.

results in [emim][dca] ( $\tilde{\nu}(\text{NO}) = 1767 \text{ cm}^{-1}$ ) with those found in water ( $\tilde{\nu}(\text{NO}) = 1810 \text{ cm}^{-1}$ )<sup>18</sup> one could even conclude a more negative binding character of NO in the case of the IL medium. Hence, the IR data for  $[\text{Fe}(\text{dca})_5\text{NO}]^{3-}$  formed in [emim][dca] as a medium supplement the UV–vis data and provide direct evidence for the reversible coordination of NO to the Fe(II) center.

The X-band EPR spectrum of the nitrosylated Fe(II) solution was measured in frozen solution at 20 K, as shown in Figure 11. The spectrum reveals at least three species present in a frozen solution. A series of low-intensity signals in the region between

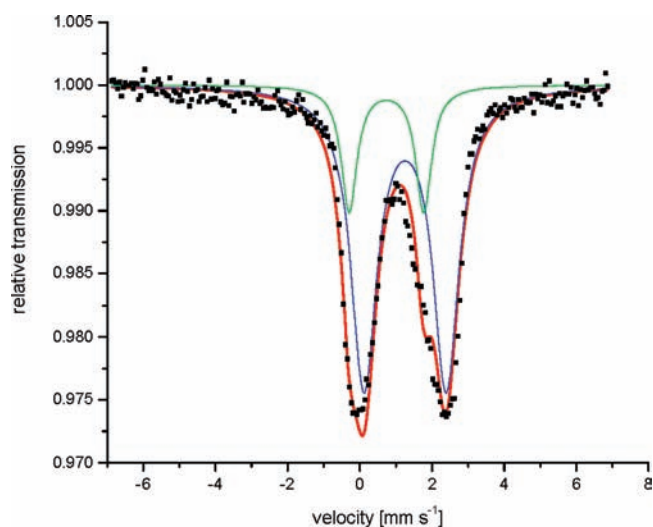


**Figure 12.** Zero-field Mössbauer spectrum of the Fe(II) nitrosyl complex in [emim][dca] at 77 K (dots) fitted with two quadrupole doublets: (a)  $\delta = 1.25 \text{ mm s}^{-1}$ ,  $|\Delta E_Q| = 2.28 \text{ mm s}^{-1}$  – residual high-spin Fe(II) species (blue). (b)  $\delta = 0.74 \text{ mm s}^{-1}$ ,  $|\Delta E_Q| = 2.07 \text{ mm s}^{-1}$  –  $\{\text{FeNO}\}^7$  species (green).

$g = 2.16$  and  $g = 2.10$  resemble those obtained for a  $\text{FeCl}_3$  solution in [emim][dca] under similar conditions. This is ascribed to small amounts of Fe(III) being present in  $\text{FeCl}_2$  as a trace impurity. Similar signals were also found in the spectrum of  $\text{FeCl}_2$  in [emim][dca], although the precursor high-spin Fe(II) ions in the IL are expected to be EPR silent, as was shown in the literature for aqueous solution.<sup>18</sup>

The very asymmetric broad signal centered at  $g \approx 1.98$  is typical for “free” NO molecules in frozen solution. The low  $g$ -value and the large width of this  $S = 1/2$  species indicate the presence of substantial spin–orbit interaction, as expected for the NO radical.

The low-field part of the spectrum, together with the signal at  $g = 2.04$ , could be assigned to the iron nitrosyl complex with  $g$ -values of 4.05, 4.05, and 2.04, which are typical for a spin quartet species ( $S = 3/2$ ) with dominating zero-field splitting,  $D \gg h\nu$  ( $0.3 \text{ cm}^{-1}$  at X-band), and vanishing rhombicity,  $E/D = 0$ . Similar spectra have been observed for solutions of  $[\text{Fe}(\text{edta})(\text{NO})]^{55}$ ,  $[(1,4,7\text{-trimethyl-1,4,7-triazacyclononane})\text{Fe}(\text{NO})(\text{N}_3)_2]^{56}$  and  $[\text{Fe}(\text{H}_2\text{O})_5\text{NO}]\text{Cl}_2^{18}$ . Hence, the subspectrum assigned to the nitrosylated iron-dca complex confirms the  $S = 3/2$  ground state of the  $\{\text{FeNO}\}^7$  core.

The zero-field Mössbauer spectrum of the nitrosylated Fe(II) solution was measured in the frozen solution at 77 K and is reported in Figure 12. The spectrum can be deconvoluted into two overlapping quadrupole doublets with an intensity ratio of  $\sim 1:4$ . The spectrum was successfully simulated by adopting two Lorentzian doublets with different line widths. The major doublet shows a very large isomer shift,  $\delta = 1.25 \text{ mm s}^{-1}$ , and a large quadrupole splitting,  $|\Delta E_Q| = 2.28 \text{ mm s}^{-1}$ , similar to the precursor  $[\text{Fe}(\text{dca})_5\text{Cl}]^{4-}$  ( $\delta = 1.30 \text{ mm s}^{-1}$  and  $|\Delta E_Q| = 2.36 \text{ mm s}^{-1}$  (see Figure S12 in the Supporting Information). These parameters were also observed in other Fe(II)-dca species and are indicative of a high-spin Fe(II) ion in an octahedral ligand environment.<sup>57</sup> Hence, the contribution (79.3%) can be assigned to nonreacted  $[\text{Fe}(\text{dca})_5\text{Cl}]^{4-}$ , which nicely agrees with that expected for a saturated NO solution and the  $K_{\text{eq}}$  value given

above. The Mössbauer parameters,  $\delta = 0.74 \text{ mm s}^{-1}$  and  $|\Delta E_Q| = 2.07 \text{ mm s}^{-1}$ , related to the second doublet are similar to those found for  $[\text{Fe}(\text{H}_2\text{O})_5\text{NO}]^{2+}$  ( $\delta = 0.76 \text{ mm s}^{-1}$  and  $|\Delta E_Q| = 2.1 \text{ mm s}^{-1}$ )<sup>18</sup> and those previously reported for  $\text{Fe}(\text{NO})\text{SO}_4(\text{aq})$  ( $\delta = 0.76 \text{ mm s}^{-1}$  and  $|\Delta E_Q| = 2.3 \text{ mm s}^{-1}$ ),<sup>58</sup> and can therefore be assigned to the nitrosyl complex  $[\text{Fe}^{\text{III}}(\text{dca})_5\text{NO}]^{3-}$ . Isomer shifts in the range of 0.63–0.78  $\text{mm s}^{-1}$  have been observed for many octahedral  $\{\text{FeNO}\}^7 S = 3/2$  complexes, as shown in the literature<sup>56</sup> and references therein.

Since the Mössbauer and EPR parameters of the resulting nitrosyl complex  $[\text{Fe}^{\text{III}}(\text{dca})_5\text{NO}]^{3-}$  closely resemble those of  $\{\text{FeNO}\}^7$  units in other well-characterized nitrosyl complexes, we infer that its electronic structure is also best described by a high-spin Fe(III) center ( $S = 5/2$ ) antiferromagnetically coupled to  $\text{NO}^-$  ( $S = 1$ ) yielding the observed spin quartet ground state ( $S_t = 3/2$ ).

## CONCLUSIONS

The results obtained demonstrate clearly that a wide range of experimental techniques can be applied in the study of chemical processes in ionic liquids (ILs), as done for conventional molecular solvents. For the very first time, we were able to perform laser flash photolysis measurements on a reaction in an IL involving the reversible binding of NO. Furthermore, we could confirm mechanistic conclusions on the basis of the interpretation of thermal and pressure activation parameters. The mechanism of the “on” and “off” reactions of the Fe(II) complex with NO is controlled by a ligand substitution processes on the metal center, as it was found for water as solvent. We observed a changeover from an interchange dissociative ( $I_d$ ) mechanism to a dissociative (D) mechanism, since the Fe(II) starting complex contained [dca] as the ligand, as a result of the coordinating properties of the IL anion [dca]. It is important to note that, although NO is a radical, it behaves as a normal nucleophile during the ligand displacement reaction, similar to the results reported in water. However, its radical nature requires a formal charge transfer process to occur in order to stabilize the nitrosyl reaction product. The IR, Mössbauer, and EPR spectra of the iron nitrosyl complex indicate that its electronic structure is best described by the presence of high-spin Fe(III) ion ( $S = 5/2$ ) antiferromagnetically coupled to  $\text{NO}^-$  ( $S = 1$ ) to yield the observed spin quartet ground state ( $S_t = 3/2$ ). Our results reveal that more attempts have to be undertaken to quantify possible mechanistic changes when a well-known reaction is performed in an IL medium. Furthermore, it will be essential to reconsider the donor strength of the anionic component of the IL in terms of possible coordination to the metal center, whereby such ILs cannot be considered as innocent solvents anymore.

## ASSOCIATED CONTENT

**S Supporting Information.** Twelve figures reporting different projections of the molecular structure, IR spectra, the absorption spectrum of  $[\text{emim}][\text{dca}]$ , absorbance changes as a function of complex concentration, Gibbs–Helmholtz plot, plot of  $\ln(K_{\text{eq}})$  versus pressure, typical flash photolysis kinetic trace, Eyring plots, plots of  $\ln(k)$  versus pressure, the Mössbauer spectrum of  $\text{FeCl}_2$  in  $[\text{emim}][\text{dca}]$ , and a table summarizing rate constants measured as a function of pressure (13 pages).

This material is available free of charge via the Internet at <http://pubs.acs.org>.

## AUTHOR INFORMATION

### Corresponding Author

\*E-mail: [vaneldik@chemie.uni-erlangen.de](mailto:vaneldik@chemie.uni-erlangen.de).

## ACKNOWLEDGMENT

The authors gratefully acknowledge financial support from the Deutsche Forschungsgemeinschaft through SPP 1191 on Ionic Liquids. A part of our research was carried out with equipment purchased with financial support of the European Regional Development Fund within the framework of the Polish Innovation Economy Operational Program (Contract No. POIG.02.01.00-12-023/08). We kindly thank Dr. Jörg Sutter, Dr. Marat Khusniyarov and Prof. Karsten Meyer for assistance with the Mössbauer spectra, and acknowledge the technical support of Susanne Hoffmann with the IR measurements.

## REFERENCES

- (1) Baker, G. A.; Baker, S. N.; Pandey, S.; Bright, F. V. *Analyst* **2005**, *130*, 800–808.
- (2) Poole, C. F. J. *Chromatogr. A* **2004**, *1037*, 49–82.
- (3) Tang, F.; Kangkang, W.; Ding, L.; Yuan, J.; Liu, Q.; Nie, L.; Yao, S. *Sep. Purif. Technol.* **2008**, *60*, 245–250.
- (4) Plechkova, N. V.; Seddon, K. R. *Chem. Soc. Rev.* **2008**, *37*, 123–150.
- (5) Maase, M. *Multiphase Homogeneous Catal.* **2005**, *2*, 560–566.
- (6) Tempel, D.; Henderson, P.; Brzozowski, J.; Pearlstein, R.; Garg, D. U.S. Patent Application Publ., Cont.-in-part of U.S. Ser. No. 948,277, 2006 (15 pp).
- (7) McNulty, J.; Cheekoori, S.; Bender, T. P.; Coggan, J. A. *Eur. J. Org. Chem.* **2007**, *9*, 1423–1428.
- (8) Daguinet, C.; Dyson, P. *Organometallics* **2006**, *25*, 5811–5816.
- (9) (a) Begel, S.; Illner, P.; Kern, S.; Puchta, R.; van Eldik, R. *Inorg. Chem.* **2008**, *47*, 7121–7132. (b) Illner, P.; Begel, S.; Kern, S.; Puchta, R.; van Eldik, R. *Inorg. Chem.* **2009**, *48*, 588–597.
- (10) (a) Muldoon, M. J.; Aki, S. N. V. K.; Anderson, J. L.; Dixon, J. K.; Brennecke, J. F. *J. Phys. Chem. B* **2007**, *111*, 9001–9009. (b) Anderson, J. L.; Dixon, J. K.; Maginn, E. J.; Brennecke, J. F. *J. Phys. Chem. B* **2006**, *110*, 15059–15062. (c) Anderson, J. L.; Dixon, J. K.; Brennecke, J. F. *Acc. Chem. Res.* **2007**, *40*, 1208–1216.
- (11) Bresme, F.; Alejandre, J. J. *Chem. Phys.* **2003**, *118*, 4134–4139.
- (12) (a) Anthony, J. L.; Anderson, J. L.; Maginn, E. J.; Brennecke, J. F. *J. Phys. Chem. B* **2005**, *109*, 6366–6374. (b) Carvalho, P. J.; Alvarez, V. H.; Marrucho, I. M.; Aznar, M.; Coutinho, J. A. P. *J. Supercrit. Fluids* **2009**, *50*, 105–111.
- (13) (a) Bara, J. E.; Gabriel, C. J.; Carlisle, T. K.; Camper, D. E.; Finotello, A.; Gin, D. L.; Noble, R. D. *Chem. Eng. J.* **2009**, *147*, 43–50. (b) Bates, E.; Mayton, R.; Ntai, I.; Davis, J. J. *Am. Chem. Soc.* **2002**, *124*, 926–927. (c) Han, X.; Armstrong, D. W. *Acc. Chem. Res.* **2007**, *40*, 1079–1086. (d) Ferguson, L.; Scovazzo, P. *Ind. Eng. Chem. Res.* **2007**, *46*, 1369–1374.
- (14) (a) Moreau, M.; Lindermayr, C.; Durner, J.; Klessig, D. F. *Physiol. Plant* **2010**, *138*, 372–383. (b) Pena-Altamira, E.; Petazzi, P.; Contestabile, A. *Curr. Pharm. Des.* **2010**, *16*, 440–450. (c) Ostrowski, A. D.; Ford, P. C. *Dalton Trans.* **2009**, *48*, 10660–10669. (d) Lundberg, J. O. *Biosci. Microflora* **2008**, *27*, 109–112. (e) Ivanovic-Burmazovic, I.; van Eldik, R. *Dalton Trans.* **2008**, *39*, 5259–5275. (f) Chiang, C.-Y.; Darensbourg, M. Y. *J. Biol. Inorg. Chem.* **2006**, *11*, 359–370. (g) Ford, P. C.; Lorkovic, I. M. *Chem. Rev.* **2002**, *102*, 993–1017. (h) Ueno, T.; Suzuki, Y.; Fujii, S.; Vanin, A. F.; Yoshimura, T. *Biochem. Pharmacol.* **2002**, *63*, 485–493. (i) Sojka, Z. *Appl. Magn. Reson.* **2000**, *18*, 71–83.

- (15) Laverman, L. E.; Wanat, A.; Oszejka, J.; Stochel, G.; Ford, P. C.; van Eldik, R. *J. Am. Chem. Soc.* **2001**, *123*, 285–293.
- (16) Wolak, M.; Stochel, G.; Zahl, A.; Schneppen sieper, T.; van Eldik, R. *J. Am. Chem. Soc.* **2001**, *123*, 9780–9791.
- (17) Culotta, E.; Koshland, D. E. *Science* **1992**, *258*, 1862–1865.
- (18) Wanat, A.; Schneppen sieper, T.; Stochel, G.; van Eldik, R.; Bill, E.; Wieghardt, K. *Inorg. Chem.* **2002**, *41*, 4–10.
- (19) Schmeisser, M.; van Eldik, R. *Inorg. Chem.* **2009**, *48*, 7466–7475.
- (20) Bonhôte, P.; Dias, A. P.; Papageorgiou, N.; Kalyanasundaram, K.; Grätzel, M. *Inorg. Chem.* **1996**, *35*, 1168–1178.
- (21) Schöffski, K. *Chem. Unserer Zeit.* **2000**, *34*, 170–175.
- (22) Unpublished results; for the general procedure used to determine the solubility of NO, see ref 23.
- (23) Wasserscheid, P.; Welton, T. *Ionic Liquids in Synthesis*; Wiley–VCH: Weinheim, Germany, 2003; p 81.
- (24) (a) Spitzer, M.; Gartig, F.; van Eldik, R. *Rev. Sci. Instrum.* **1988**, *59*, 2092–2093. (b) Fleischmann, K. F.; Conze, G. E.; Stranks, R. D.; Kelm, H. *Rev. Sci. Instrum.* **1974**, *45*, 1427–1430.
- (25) Nova Werke AG, Vogelsangstrasse 24, CH-8307 Effretikon, Switzerland.
- (26) SADABS 2.06; Bruker AXS, Inc.: Madison, WI, 2009.
- (27) SHELXTL NT 6.12; Bruker AXS, Inc.: Madison, WI, 2002.
- (28) (a) Das, S.; Bhar, K.; Fun, H.-K.; Chantapromma, S.; Ghosh, B. K. *Inorg. Chim. Acta* **2010**, *363*, 784–792. (b) Sarkar, B. N.; Bhar, K.; Chattopadhyay, S.; Das, S.; Mitra, P.; Ghosh, B. K. *J. Mol. Struct.* **2010**, *963*, 35–40. (c) Ma, K.; Shi, Q.; Hu, M.; Cai, X.; Huang, S. *Inorg. Chim. Acta* **2009**, *362*, 4926–4930. (d) Mautner, F. A.; Mikuriya, M.; Ishida, H.; Sakiyama, H.; Louka, F. R.; Humphrey, J. W.; Massoud, S. S. *Inorg. Chim. Acta* **2009**, *362*, 4073–4080. (e) Das, A.; Marschner, C.; Cano, J.; Baumgartner, J.; Ribas, J.; El Fallah, M. S.; Mitra, S. *Polyhedron* **2009**, *28*, 2436–2442. (f) Liu, H.; Tian, J.-L.; Kou, Y.-Y.; Gu, W.; Feng, L.; Yan, S.-P.; Liao, D.-Z. *Anorg. Allg. Chem.* **2008**, *634*, 1565–1569.
- (29) Kohout, J.; Jager, L.; Hvastijova, M.; Kozisek, J. *J. Coord. Chem.* **2000**, *51*, 169–218.
- (30) Genre, C.; Jeanneau, E.; Bousseksou, A.; Luneau, D.; Borshch, S. A.; Matouzenko, G. S. *Chem.—Eur. J.* **2008**, *14*, 697–705.
- (31) Ortega-Villar, N.; Thompson, A. L.; Munoz, M. C.; Ugalde-Saldivar, V. M.; A. E. Goeta, A. E.; Moreno-Esparza, R.; Real, J. A. *Chem.—Eur. J.* **2005**, *11*, 5721–5734.
- (32) Triki, S.; Thetiot, F.; Galan-Mascaros, J.-R.; Sala Pala, J.; Dunbar, K. R. *New J. Chem.* **2001**, *25*, 954–958.
- (33) Batten, S. R.; Murray, K. S. *Coord. Chem. Rev.* **2003**, *246*, 103–130.
- (34) (a) Batten, S. R.; Jensen, P.; Kepert, C. J.; Kurmoo, M.; Moubaraki, B.; Murray, K. S.; Price, D. J. *J. Chem. Soc. Dalton Trans.* **1999**, *17*, 2987–2997. (b) Jensen, P.; Batten, S. R.; Fallon, G. D.; Moubaraki, B.; Murray, K. S.; Price, D. J. *Chem. Commun.* **1999**, *2*, 177. (c) Mohamadou, A.; van Albada, G. A.; Kooijman, H.; Wiezcorek, B.; Spek, A. L.; Reedijk, J. *New J. Chem.* **2003**, *27*, 983–988. (d) Jurgens, B.; Irran, E.; Hoppe, H. A.; Schnick, W. Z. *Anorg. Allg. Chem.* **2004**, *630*, 219–223.
- (35) Tonzing, D. S.; Batten, S. R.; Murray, K. S. *J. Mol. Struct.* **2006**, *796*, 63–68.
- (36) Batten, S. R.; Bjernemose, J.; Jensen, P.; Leita, B. A.; Murray, K. S.; Moubaraki, B.; Smith, J. P.; Tofflund, H. *Dalton Trans.* **2004**, 3370–3375.
- (37) Das, A.; Jana, A. D.; Seth, S. K.; Dey, B.; Choudhury, S. R.; Kar, T.; Mukhopadhyay, S.; Singh, N. J.; Hwang, I.-C.; Kim, K. S. *J. Phys. Chem. B* **2010**, *114*, 4166–4170; and literature thereof.
- (38) Qin, D.-B.; Jin, L.-H.; Gu, S.-J.; Zhang, H.-X. *Acta Crystallogr., Sect E: Struct. Rep. Online* **2006**, *62*, o4176.
- (39) Yoshida, Y.; Muroi, K.; Otsuka, A.; Saito, G.; Takahashi, M.; Yoko, T. *Inorg. Chem.* **2004**, *43*, 1458–1462.
- (40) Holleman, A. F.; Wieberg, E., Eds. *Lehrbuch der Anorganischen Chemie*; Walter de Gruyter: Berlin, New York, 1995.
- (41) Wang, F.; Wu, X.-Y.; Zhao, Z.-G.; Zhang, Q.-S.; Xie, Y.-M.; Yu, R.; Lu, C.-Z. *Inorg. Chim. Acta* **2010**, *363*, 1320–1324.
- (42) Köhler, H.; Kolbe, A.; Lux, G. Z. *Anorg. Allg. Chem.* **1977**, *428*, 103–112.
- (43) (a) van Albada, G. A.; Mutikainen, I.; Turpeinen, U.; Reedijk, J. *Inorg. Chem. Commun.* **2006**, *9*, 441–443. (b) Ortega-Vallar, N.; Thompson, A. L.; Munoz, M. C.; Ugalde-Saldivar, V. M.; Goeta, A. E.; Moreno-Esparza, R.; Real, J. A. *Chem.—Eur. J.* **2005**, *11*, 5721–5734. (c) Zhang, L.; Shi, L.; Chen, Z. *Inorg. Chem.* **2003**, *42*, 633–640. (d) Martin, S.; Barandika, G.; Ezpeleta, J. M.; Cortes, R.; Ruiz de Larramendi, J. I.; Lezama, L.; Rojo, T. *J. Chem. Soc., Dalton Trans.* **2002**, 4275–4280. (e) Manson, J. L.; Arif, A. M.; Miller, J. S. *J. Mater. Chem.* **1999**, *9*, 979–983.
- (44) Marshall, S. R.; Rheingold, A. L.; Dawe, L. N.; Shum, W. W.; Kitamura, C.; Miller, J. S. *Inorg. Chem.* **2002**, *41*, 3599–3601.
- (45) Manson, J. L.; Arif, A. M.; Incarvito, C. D.; Liable-Sands, L. M.; Rheingold, A. L.; Miller, J. S. *J. Solid State Chem.* **1999**, *145*, 369–378.
- (46) Mrozinski, J.; Kohout, J.; Hvastijova, M.; Köhler, H. *Transition Met. Chem.* **1986**, *11*, 481.
- (47) Hamza, A. S. M.; Zou, X.; Banka, R.; Brown, K. L.; van Eldik, R. *Dalton Trans.* **2005**, *4*, 782–787.
- (48) (a) van Eldik, R. *Coord. Chem. Rev.* **2007**, *251*, 1649–1662. (b) Harwood, L. M. *Angew. Chem., Int. Ed. Engl.* **2003**, *42*, 4852. (c) van Eldik, R.; Hubbard, C. D. *Chem. Z.* **2000**, *34*, 306–317. (d) van Eldik, R.; Hubbard, C. D. *Chem. Unserer Zeit.* **2000**, *34*, 240–252.
- (49) (a) The partial molar volume was calculated from the ionic radius of chloride given in: Aylward, G. H.; Findlay, T. J. V. *Datensammlung Chemie in SI-Einheiten*; Verlag Chemie: Weinheim, Germany, 1981. (b) The partial molar volume was obtained from density measurements reported in: Millero, F. J. in Horne, R. A., Ed. *Water and Aqueous Solutions: Structure, Thermodynamics and Transport Processes*, Wiley–Interscience: London, 1972; Chapter 13.
- (50) Plyasunov, A. V.; O’Connell, J. P.; Wood, R. H. *Geochim. Cosmochim. Acta* **2000**, *64*, 495–512.
- (51) Schneppen sieper, T.; Wanat, A.; Stochel, G.; Goldstein, S.; Meyerstein, D.; van Eldik, R. *Eur. J. Inorg. Chem.* **2001**, *9*, 2317–2325.
- (52) (a) Kurtikyan, T. S.; Ford, P. C. *Coord. Chem. Rev.* **2008**, *252*, 1486–1496. (b) Machura, B. *Coord. Chem. Rev.* **2005**, *249*, 2277–2307. (c) Mingos, D. M. P.; Sherman, D. J. *Adv. Inorg. Chem.* **1989**, *34*, 293. (d) McCleverty, J. A. *Chem. Rev.* **1979**, *79*, 53.
- (53) Feelisch, M.; Stamler, J., Eds. *Methods in Nitric Oxide Research*; John Wiley & Sons, Ltd.: West Sussex, U.K., 1996; Chapter 29.
- (54) Schneppen sieper, T.; Finkler, S.; Czap, A.; van Eldik, R.; Heus, M.; Nieuwenhuizen, P.; Wreesmann, C.; Abma, W. *Eur. J. Inorg. Chem.* **2001**, 491–501.
- (55) (a) Brown, C. A.; Pavlosky, M. A.; Westre, T. E.; Zhang, Y.; Hedman, B.; Hodgson, K. O.; Solomon, E. I. *J. Am. Chem. Soc.* **1995**, *117*, 715–732. (b) Westre, T. E.; Di Cicco, A.; Filipponi, A.; Natoli, C. R.; Hedman, B.; Solomon, E. I.; Hodgson, K. O. *J. Am. Chem. Soc.* **1994**, *116*, 6757–6768.
- (56) Hauser, C.; Glaser, T.; Bill, E.; Weyhermüller, T.; Wieghardt, K. *J. Am. Chem. Soc.* **2000**, *122*, 4352–4365.
- (57) van der Werff, P. M.; Batten, S. R.; Jensen, P.; Moubaraki, B.; Murray, K. S.; Cashion, J. D. *Crystal Growth Des.* **2004**, *4*, 503–508.
- (58) Mosbaek, H.; Poulsen, K. G. *Acta Chem. Scand.* **1971**, *25*, 2421.

## NOTE ADDED AFTER ASAP PUBLICATION

This paper was published on the Web on March 23, 2011, with a minor error in the sentence below the caption of Figure 8. The corrected version was reposted on March 28, 2011.